J. Earth Syst. Sci. (2025)134 119
https://doi.org/10.1007/s12040-025-02559-5

Characterization of wall rock alteration and its implications for graphite mineralization in the Kahatagaha–Kolongaha vein graphite deposits, Sri Lanka

T C Senevirathna[1,3], P L Dharmapriya[2,*], N W B Balasooriya[2], H M T G A Pitawala[1,2], H W M A C Wijayasinghe[3], Medhavi Abeysinghe[3] and K Sajeev[4]

[1]*Postgraduate Institute of Science, University of Peradeniya, Peradeniya, Sri Lanka.*
[2]*Department of Geology, University of Peradeniya, Peradeniya, Sri Lanka.*
[3]*National Institute of Fundamental Studies, Kandy, Sri Lanka.*
[4]*Center for Earth Sciences, Indian Institute of Science, Bangalore, India.*
[*]*Corresponding author. e-mail: prasannad@sci.pdn.ac.lk*

MS received 24 October 2024; revised 8 February 2025; accepted 17 February 2025

Sri Lankan vein graphite deposits are renowned for their high purity and crystal structure, making them economically valuable. Previous studies have focused on their origins and economic potential, but the alteration of wall rock during graphite mineralization and the role of hydrothermal fluids have been less explored. Understanding these fluid-rock interactions is crucial for assessing vein graphite purity. This study elucidates these processes through petrological analysis of host rocks from the Kahatagaha–Kolongaha underground mine. We examined field relationships, vein textures, mineralogy, and petrological attributes of wall rock alterations to determine the influence of hydrothermal fluids on wall rock modifications and their impact on graphite vein purity. Significant wall rock alterations were observed due to hydrothermal fluids, involving changes in mineralogical composition and texture. Mildly acidic conditions from CO_2 and H_2O interactions facilitated feldspar dissolution, releasing elements contributing to antiperthitization and myrmekite formation. These alterations produced biotite, titanite, two feldspars, and calcite, affecting graphite purity. Our findings align with previous research indicating a retrograde origin following major tectonic events and large-scale folding of the Sri Lankan basement.

Keywords. Vein graphite; hydrothermal fluid; wall-rock alteration; albitization; Sri Lanka.

1. Introduction

Hydrothermal fluids sourced from diverse reservoirs, including subducted oceanic crust, metamorphic fluids, and magmatic or metamorphic sources, are fundamental in ore deposit genesis (Kawagucci 2015; Sillitoe 2015; Patten *et al.* 2017). These fluids constitute complex mixtures of gasses and aqueous solutions containing highly fusible gasses, simple ions, complex ions, dissolved bases, and precious metals (Pirajno 2012; Keith *et al.* 2018). They facilitate the dissolution, transportation, and deposition of ore-forming elements under high temperatures and pressures, with ore-forming metals mobilizing from the source as fluids and conveyed to deposition sites as stable complexes (Pirajno 1992; Ding *et al.* 2018). Hydrothermal veins, acting as conduits for mineral-laden fluids, initiate a series of chemical reactions as they traverse fractures and faults within the Earth's crust,

Published online: 26 May 2025

gradually depositing valuable minerals along conduit walls (Barnes 1997). This process influences both the mineralogical composition of surrounding rocks and imparts distinct signatures to resulting vein deposits (Lowenstern *et al.* 2015).

The mineralization mechanisms of vein graphite deposits are commonly attributed to the transportation of carbon-bearing hydrothermal fluids through fracture systems within host rocks (Touzain *et al.* 2010; Luque *et al.* 2012; Rumble 2014). The carbon isotope composition of these graphite exhibits a broad range, suggesting potential sources, including organic matter, carbonates, and igneous carbon from the mantle (Wilson *et al.* 1995; Binu-Lal *et al.* 2003; Shirey *et al.* 2013).

The vein graphite deposits of Sri Lanka are situated within Precambrian high-grade metamorphic terrain dominated by granulite facies rocks. These deposits are known for their high purity (∼95–99% pure carbon), crystallinity, large reserves, and mode of occurrence, and have been extensively studied for their genesis and economic significance (Hapuarachchi 1977; Katz 1987; Dissanayake 1994; Kehelpannala 1999; Touzain *et al.* 2010). These studies illustrated that Sri Lankan vein graphite deposits have been attributed to both syngenetic and epigenetic processes throughout history, given their high purity and crystallinity (Erdosh 1970; Hapuarachchi 1977; Dobner *et al.* 1978; Wijayananda and Jayawardana 1983; Katz 1987; Silva 1987; Dissanayake 1994; Kehelpannala 1995; Binu-Lal *et al.* 2003; Touzain *et al.* 2010; Hewathilaka *et al.* 2015). Despite their economic significance, limited studies have focused on understanding fluid flow processes and factors governing the formation of distinct graphite varieties (e.g., Touzain *et al.* 2010; Hewathilaka *et al.* 2015). Additionally, there have been few attempts to study wall rock alteration during graphite mineralization (e.g., Silva 1987; Touret *et al.* 2019), and modification of the hydrothermal fluid contributed to vein graphite formation, heavily influencing the purity of graphite veins. Meanwhile, only a handful of attempts have been made to evaluate the temperature conditions at which graphite mineralization had taken place (e.g., Touret *et al.* 2019). A comprehensive understanding necessitates interpreting field relationships, vein textures, mineralogy, and petrological characterization of wall-rock alteration features to illuminate the evolution and chemical fluid-wall rock interaction history of these deposits. Moreover, the scarcity of geochronological information has fueled debates about accurately comprehending the dynamics of hydrothermal graphite mineralization in correlation with the evolution of Sri Lankan basement rocks.

The study conducted a comprehensive petrological analysis of the host rock of vein graphite, focusing on samples from the Kahatagaha–Kolongaha underground mine in Sri Lanka. This research aimed to provide insights into several key aspects of vein graphite formation. These include determining the probable composition of the initial fluid responsible for vein graphite formation and establishing the chronological sequence of vein graphite mineralization in Sri Lanka. These insights contribute to a better understanding of vein graphite formation processes and the geological history of the region.

2. General geology of Sri Lanka and previous studies on Sri Lankan vein graphite

2.1 *General geology of the Sri Lankan basement*

The Proterozoic basement of Sri Lanka is traditionally subdivided into four units (figure 1): the Wanni Complex (WC), Kadugannawa Complex (KC), Highland Complex (HC), and Vijayan Complex (VC), based on Nd model ages and zircon U–Pb dating (Milisenda *et al.* 1988, 1994; Kröner *et al.* 1991; Liew *et al.* 1991). The Nd-model ages obtained from the Western Complex (WC) range from 2000 to 1000 million years ago (Ma), as reported by Milisenda *et al.* (1988, 1994). The WC comprises a diverse array of rock compositions, including granitic, granodiorite, monzonite, tonalite, charnockitic, and enderbitic rocks, reflecting variations in protolith chemistry (Pohl and Emmermann 1991). The metasedimentary rocks of the WC are primarily situated in the eastern and southeastern regions of the complex, adjacent to the western margin of the HC (Kehelpannala 1997). In the western region of the WC, less deformed granites predominate, with examples such as the unmetamorphosed post-tectonic K-feldspar-rich granite of Thonigala (Hölzl *et al.* 1991; Cooray 1994) and carbonatite at Eppawala and Kawisigamuwa (e.g., Pitawala and Lottermose 2012; Madugalla *et al.* 2014; Su *et al.* 2022). The peak metamorphic conditions within the WC are estimated to have reached temperatures of 700–830°C and pressures of 5–7 kbar (Raase and Schenk 1991; Santosh *et al.* 2014; Hirayama *et al.*

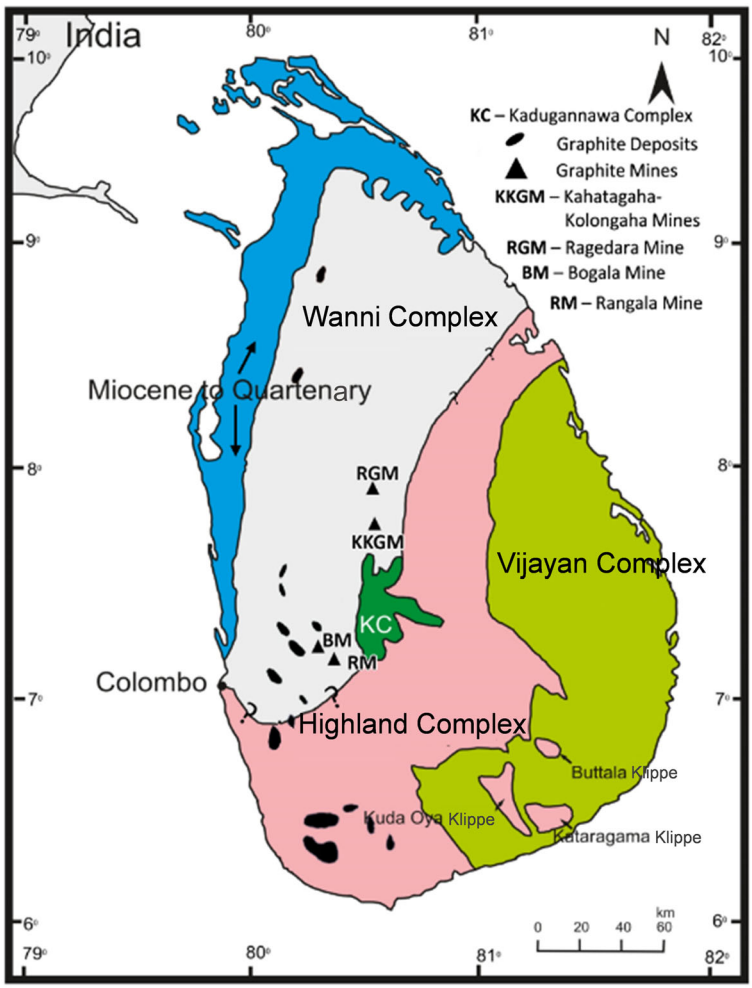

Figure 1. A map showing the lithotectonic subdivision of Sri Lanka (modified after Cooray 1994) and the locations of major vein graphite deposits in Sri Lanka.

2020; Jayathilaka *et al.* 2022). The intrusion ages of Wanni gneisses typically fall within the ranges of ~1100–920 Ma, 800–750 Ma, and around 580 Ma (Hölzl *et al.* 1994; Kröner *et al.* 1994, 2003; Santosh *et al.* 2014; He *et al.* 2016). Peak metamorphism is inferred to have occurred around 590–540 Ma based on U–Pb zircon geochronology (Hölzl *et al.* 1994; Kröner *et al.* 1994, 2003; Santosh *et al.* 2014; He *et al.* 2016). Several graphite deposits are situated in the eastern part of the Wanni Complex, near the northwest boundary of the Highland Complex (e.g., Wijayananda and Jayawardana 1983; Katz 1987; Silva 1987).

The HC comprises granulite facies metasedimentary and metaigneous rocks, including quartzites, marbles, calcsilicates, pelitic gneisses, charnockites, and orthogneisses (Cooray 1984, 1994; Mathavan and Fernando 2001; Dharmapriya *et al.* 2020). Nd model ages for the HC range from 3400–2000 Ma (Milisenda *et al.* 1988, 1994). The Kadugannawa Complex (KC) is exposed within doubly plunging upright folds around the Kadugannawa area in central Sri Lanka, historically referred to as 'Arenas' (Vitanage 1972; Almond 1991). Nd-model dating of the KC suggests ages spanning from 1800 to 1100 Ma ago (Milisenda *et al.* 1988, 1994). The predominantly upper amphibolite facies Vijayan Complex (VC) yields Nd-model ages ranging between 3300 and 1100 Ma (Milisenda *et al.* 1988, 1994; Malaviarachchi *et al.* 2021). This Complex is primarily composed of microcline-bearing granitic gneisses, augen gneisses, migmatites, and hornblende-biotite gneisses (Cooray 1984; Kehelpannala 1997; Mathavan and Fernando 2001; Kröner *et al.* 2013).

Various researchers, including Berger and Jayasinghe (1976), Yoshida *et al.* (1990), Kriegsman (1991, 1994, 1995), Kehelpannala (1993, 1997, 2003), Kleinschrodt (1994, 1996), and

Tani and Yoshida (1996), have explored the deformation history of the Sri Lankan basement. Berger and Jayasinghe (1976) proposed three deformation phases, suggesting that D1 and D2 formed major lineation and foliation (L–S fabric), including primary compositional layering, while D3 mainly led to large-scale upright fold formation. Kriegsman (1991, 1994) noted the development of steep, high-T shear zones during the late D3 stages. Furthermore, Kehelpannala (1997) suggested that the Highland Complex (HC) and Wanni Complex (WC) experienced six phases of ductile deformation. At the same time, D1 to D2 resemble earlier descriptions. In contrast, many minor and large-scale recumbent isoclinal folds (F3) were produced during D3, and D4 resulted in the development of large, gentle, nearly E–W trending upright folds. D5 contributed to large-scale upright folds (F5). D6 was associated with local refolding of the F5 folds.

2.2 *A brief overview of previous studies on vein graphite in Sri Lanka*

Previous studies identified four crystalline forms of Sri Lankan vein graphite: needle, flake, spherulitic, and powder (fine-grained graphite) (Erdosh 1970; Cooray 1984; Katz 1987; Silva 1987). Typically, individual veins consist of a single form, arranged in parallel sheets, with medium to coarse-grained crystals such as flake or needle graphite (Erdosh 1970; Katz 1987). Later research refined this classification by highlighting differences in crystallinity, purity, microstructure, and origin based on graphite morphology (Kehelapannala 1993; Balasooriya *et al.* 2002; Touzain *et al.* 2010; Hewathilake *et al.* 2015). The formation of vein graphite is attributed to carbon-bearing hydrothermal fluids moving through fractures in host rocks (Touzain *et al.* 2010; Luque *et al.* 2012; Rumble 2014). These fluids, with varying carbon isotope compositions from sources like organic matter, carbonates, and mantle-derived carbon, undergo hydrothermal redox reactions between CO_2 and methane, facilitating graphite formation (Touzan *et al.* 2010; Luque *et al.* 2012; Rumble 2014). Graphitization is primarily influenced by temperature, metamorphic duration, and rock type, with carbon deposition from CO_2 or CH_4 in supercritical fluids driven by cooling and fluid-rock interactions (Wada *et al.* 1994; Huizenger 2011).

The origin of Sri Lankan graphite is explained by two models: syngenetic graphite formed during prograde metamorphism and epigenetic graphite from carbon-rich fluids linked to igneous activity. Graphitization is influenced by temperature, metamorphic duration, and lithology, with carbon existing as CO_2 or CH_4 in supercritical fluids and deposition driven by cooling and fluid-rock interactions (Luque *et al.* 1998, 2014). Touret *et al.* (2019) proposed that mantle-derived CO_2, stored in the lower crust during Gondwana's formation, was released during decompression, forming graphite veins in Sri Lanka, similar to quartz-carbonate shear zones in granulite terranes. The specific formation of graphite or quartz-carbonate veins depends on prevailing chemical conditions.

Graphite veins are often localized in anticlinal structures, indicating mineralization due to structural weaknesses during the folding of metasedimentary rocks (Silva 1987). Katz (1987) suggested that CO_2-rich fluids under low fO_2 conditions caused hydraulic fracturing and vein graphite formation. Kehelpannala (1995) argued this mineralization is younger (550–475 Ma) and unrelated to peak metamorphism.

Touret *et al.* (2019) suggested graphite formed during rapid decompression that uplifted high-grade metamorphic rocks. The host rocks for these graphite deposits primarily include pelitic and charnockitic gneisses, which often contain disseminated flake graphite. Hydrothermal alteration near graphite veins is evident, with hydrous and chlorine-rich minerals such as biotite, chlorite, hornblende, and scapolite present (Silva 1987; Kehelpannala 1999; Touret *et al.* 2019). This alteration of wall rock during mineralization is a key factor contributing to the impurities found in vein graphite (Silva 1987; Kehelpannala 1999; Touret *et al.* 2019).

3. Sample description and field relations

The Kahatagaha–Kolongaha underground mine (figure 1) in Sri Lanka primarily operates as a vein graphite deposit, located about 32 km north–northwest of Kandy, within the Wanni Complex (see figure 1). The area surrounding Kahatagaha comprises quartzite, quartzofeldspathic gneisses, garnet–cordierite–biotite, sillimanite-bearing gneisses, granitic gneisses, charnockites, and biotite-gneisses (Geology Map of Geological Survey and Mines

Bureau 1996, Sheet No. 14). Within this mine, graphite veins intersect granulite facies metamorphic rocks, including charnockites and garnet-biotite gneisses. The orientation of graphite-bearing veins is predominantly east–west, with a dip direction towards the south (Touret *et al.* 2019). The thickness of graphite veins typically ranges from a few millimeters to several decimeters (see figure 2a, b). However, veins occasionally exceed a thickness of 1 m (see figure 2c). Their horizontal length varies from a few decimeters to tens of meters, with extensions over 75 m (Kehelpannala 1999). Within certain graphite veins, typical vein-type quartz devoid of evidence for ductile deformation is present (see figure 2d), along with clusters of precipitated calcite (see figure 2e) and euhedral to subhedral or thin films of pyrite (see figure 2f) as visible gangue minerals. In some areas, a very thin layer of wall rock can be observed between graphite layers, forming a sandwich-like structure (see figure 2c).

For the study of wall rock alteration, samples of orthopyroxene- and garnet-bearing granitic gneiss (garnet-bearing charnockite) were collected from the Kahatagaha mine at a depth level of 345 m (1132 feet). Samples were collected as a series from the host rock-vein contact of relatively large graphite veins (with thicknesses varying from 0.5 cm) to ∼1 m away from the graphite veins.

Samples collected from ∼100 to 80 cm away from graphite veins (KGK/1132/1 – see square 1 in figure 3a, b, c) contain garnet, xenomorphic quartz, two feldspars, and altered orthopyroxene, ranging in size from 0.25 to 1 cm. Coarse-grained garnet often exhibits a dark rim. Acicular biotite flakes are

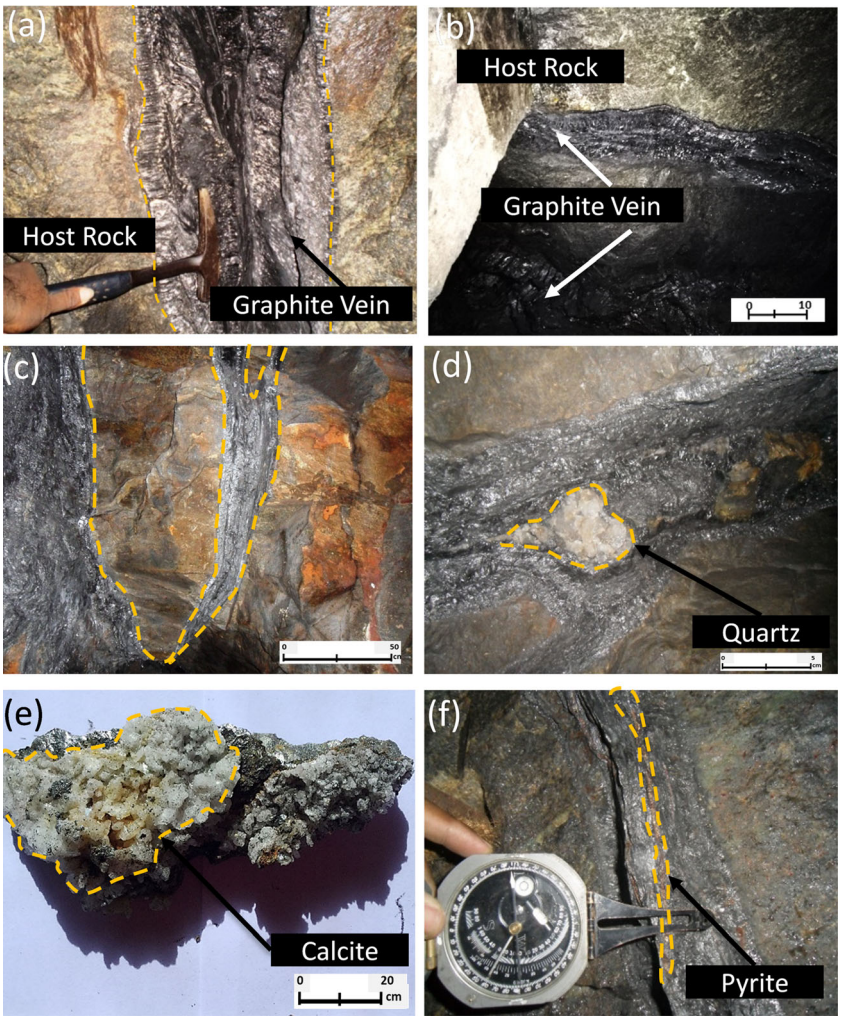

Figure 2. Some field occurrences of graphite veins nature of the graphite veins: (**a**), (**b**), and (**c**) various sizes crosscutting graphite veins in the host rocks (in (c) a fragment of host rock sandwiched among graphite veins), (**d**) vein quartz fragment within the graphite vein, (**e**) precipitated cluster of calcites collected from a graphite vein, and (**f**) thin pyrite vein associated with vein graphite.

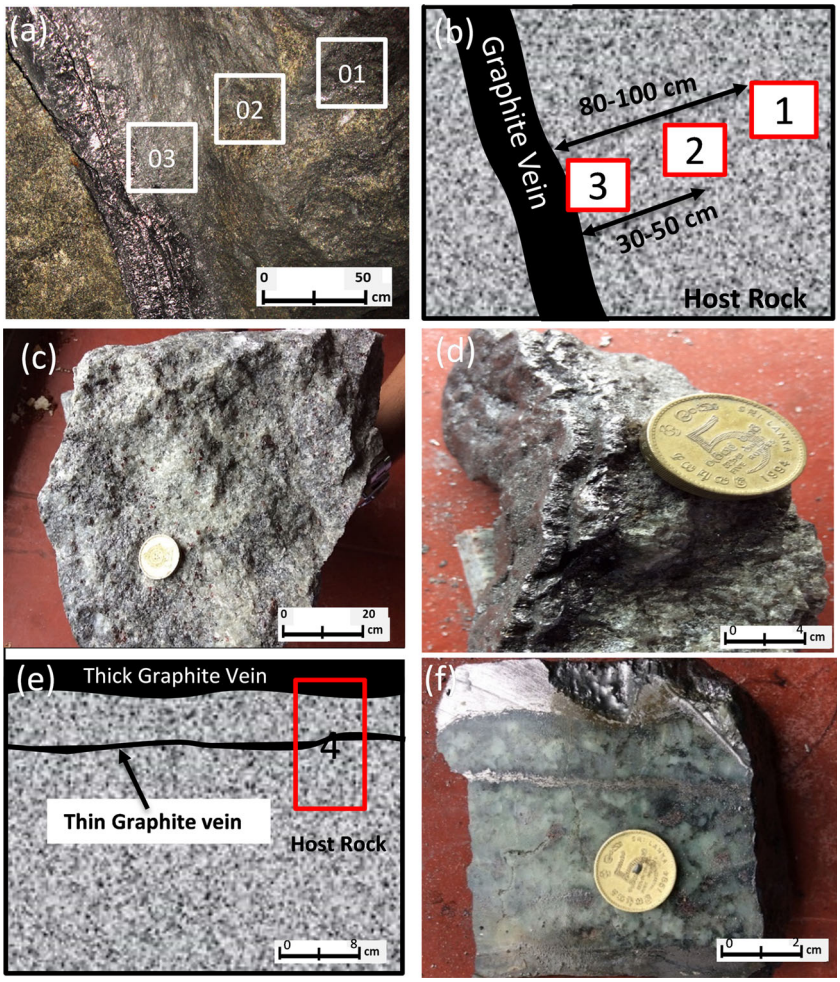

Figure 3. Relation with the graphite vein and collected samples for this study: (**a**) Sampling position of host rocks KGK/1132/1 (square 1), KGK/1132/2 (square 2), and KGK/1132/3 (square 3), (**b**) a sketch showing sampling position of the host rock KGK/1132/1 (square 1), KGK/1132/2 (square 2), and KGK/1132/3 (square 3), (**c**) collected hand specimen of KGK/1132/1, (**d**) collected hand specimen of KGK/1132/2, (**e**) a sketch showing sampling position of the host rock KGK/1132/4, and (**f**) collected hand specimen of KGK/1132/4.

observed as irregular laths or disseminated grains. Occasionally, minor disseminated graphite flakes are also present. Sample KGK/1132/2 was obtained ∼30 to 50 cm away from the main vein (see square 2 in figure 3a, b). These samples contain relatively narrow graphite veins, likely derived from the thicker main vein. The mineralogy of these hand specimens closely resembles that of KGK/1132/1. Samples KGK/1132/3 were collected adjacent to the main relatively thick (50 cm) graphite vein (see square 3 in figure 3a, b, d). They contain relatively thin graphite veins (ranging from 0.5 to 3 cm) oriented approximately parallel to the main vein. Additionally, samples of garnet-bearing mafic granulites (KGK/1132/4, figure 3e, f) occurring as dislocated layers within host rock, consisting of orthopyroxene and garnet-bearing granitic gneiss were collected at a depth of 1132 feet next to an ∼45-cm-thick graphite vein.

4. Petrography

More than 20 petrographic thin sections were prepared at the Petrological Laboratory, National Institute of Fundamental Studies, Kandy, Sri Lanka. Detailed petrographic observations were conducted using Zeiss Primotech polarizing microscopes at the Department of Geology, University of Peradeniya, Sri Lanka. Photomicrographs of the minerals were captured using the same microscope.

4.1 *Samples from location 100–80 cm adjacent to graphite veins (sample KGK/1132/1)*

The matrix of KG/1132/1 comprises xenomorphic medium to coarse-grained garnet (0.3–0.7 cm), hypidiomorphic to xenomorphic fine- to medium-grained orthopyroxene, quartz, orthoclase,

and plagioclase as major mineral constituents. Randomly oriented acicular biotite and hypidiomorphic medium-grained (∼0.25–0.4 cm) antiperthite, as well as xenomorphic ilmenite, are present as minor mineral phases. Disseminated graphite (figure 4a), apatite, and zircon are present as accessory phases. Chlorite, calcite, sericite, and rutile are observed as overprinting products after orthopyroxene and biotite. The orthopyroxene and plagioclase in this rock provide evidence for at least two generations: (a) fine to medium xenomorphic orthopyroxene (Opx_1) and plagioclase (Pl1) in the matrix (figure 4b, c) are part of the peak metamorphic assemblage of the rock, and (b) a corona of orthopyroxene (Opx_2) and plagioclase (Pl_2) after garnets (figure 4d), which originated during the retrogression of garnet breakdown.

Quartz, plagioclase, and orthoclase in the matrix exhibit slightly irregular grain boundaries, representing a granoblastic interlobate texture (see figure 4e, f). Antiperthite frequently comprises tiny orthoclase rods oriented along a single direction in host plagioclase (figure 4f). Occasionally, exsolved orthoclase blebs are also present (figure 4g). In some microdomains, plagioclase grains are partly replaced by secondary calcite and sericite. Disseminated grains of biotite and chlorite frequently overprint the matrix orthopyroxenes (figure 4b, c). Garnet also provides textural evidence for at least two generations. Medium to coarse garnet grains containing quartz, biotite, orthoclase, plagioclase, and ilmenite ± rutile as inclusion phases indicate possible garnet formation reaction (1), such as:

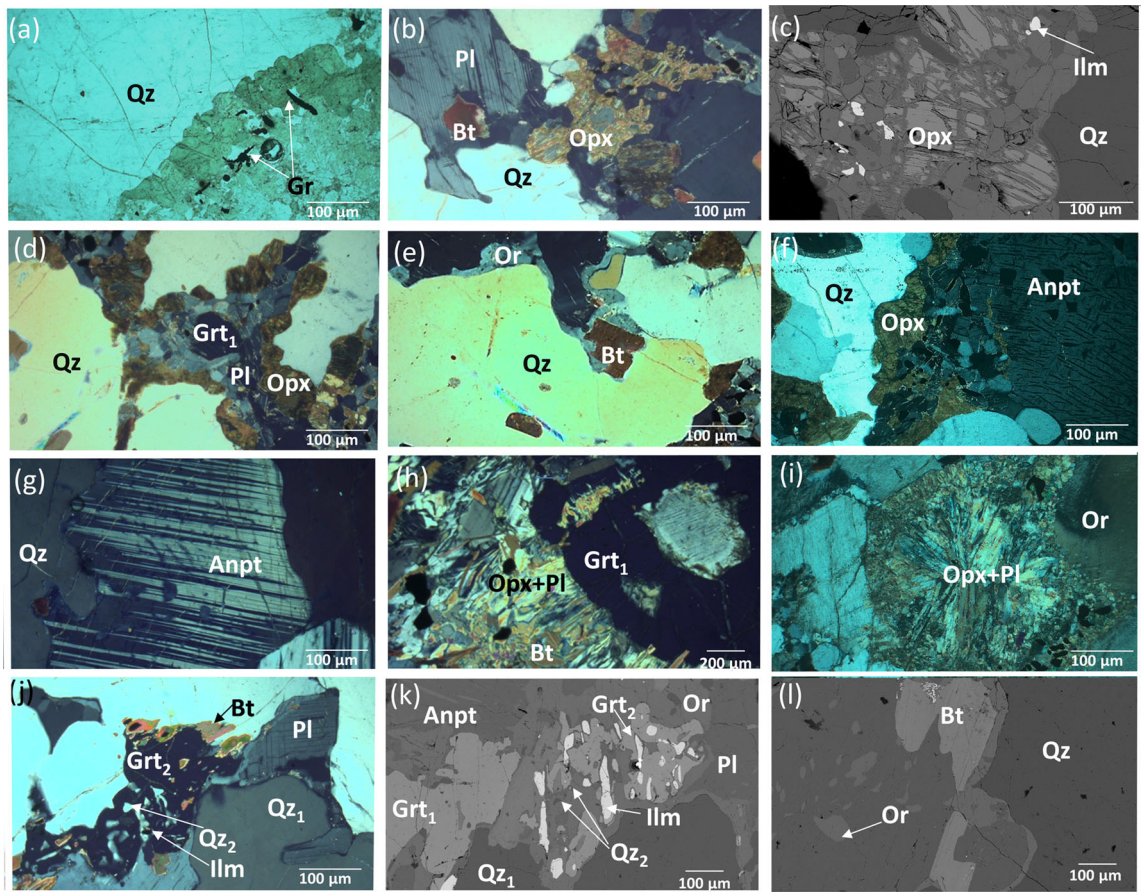

Figure 4. Petrography of sample KGK/1132/1. (**a**) The occurrences of disseminated graphite in the matrix, (**b**) chloritized coarse orthopyroxene (Opx_1), (**c**) backscattered electron image showing a coarse partial chlorites orthopyroxene (Opx_1) grain, (**d**) medium size orthopyroxene (Opx_2) + plagioclase (Pl_2) moat after garnet, (**e**) matrix quartz and feldspar showing granoblastic interlobate texture, (**f**) a coarse antiperthite grain containing exsolved orthoclase rods, (**g**) a coarse antiperthite grain containing orthoclase blabs, (**h**) orthopyroxene (Opx_2) + plagioclase (Pl_2) symplectite after coarse garnet (Grt_1), (**i**) orthopyroxene (Opx_2) + plagioclase (Pl_2) symplectite pseudomorph after garnet, (**j**) fine grain garnet containing tiny quartz inclusion associated with ilmenite and plagioclase, (**k**) BSE image showing fine grain garnet containing tiny quartz inclusion associated with ilmenite and plagioclase, (**l**) disseminate biotite grains in the matrix. Mineral abbreviations: Qz – quartz, Gr – graphite, Pl – plagioclase, Opx – orthopyroxene, Ilm – ilmenite, Or – orthoclase, Anpt – antiperthite.

$$Bt + Pl + Qz \rightarrow Grt_1 + Or + V. \quad (1)$$

The majority of Grt_1 was broken down, producing orthopyroxene–plagioclase corona (see figure 4g, h), indicating the retrograde garnet breakdown reaction (2):

$$Grt_1 + Qz \rightarrow Opx_2 + Pl_2. \quad (2)$$

In these coronas, Opx_2 and Pl_2 frequently occur as symplectite (see figure 4h). Occasionally, the outer margin of the corona contains the Opx_2–Pl_2 moat; the inner part of the same corona contains the Opx_2–Pl_2 symplectite. Later, these moats and symplectites experience intense alteration. Vermicular orthopyroxene grains were overprinted by biotite or chlorite (see figure 4h). Occasionally pseudomorphic orthopyroxene + plagioclase symplectite after garnet can also be observed (see figure 4i).

In some local domains, fine-grained skeletal garnet grains are frequently present alongside plagioclase, quartz, and iron ore (mainly ilmenite; see figure 4j, k). These garnet grains intergrow with fine-grained plagioclase ± quartz, indicating possible reaction (3) like:

$$Ilmenite + Pl_1 \rightarrow Grt_2 + Qz_2. \quad (3)$$

However, reaction (3) is difficult to chemically balance due to the lack of the Ti-rich phase that has been produced as a product (Perera 1987). Some of Grt_2 also has broken down, forming Opx_2–Pl_2 moats via reaction (2). Occasionally, Grt_2 is partially overprinted by biotite (figure 4j). Randomly oriented disseminated biotite grains are present in the matrix (figure 4b, e, l). Petrographic evidence indicates that the possible peak metamorphic assemblage of the rock consisted of Grt_1–Pl_1–Opx_1–Or–Qz_1–Ilm.

4.2 *Sample from surrounding (30–50 cm) graphite veins (KGK/1132/2)*

This sample exhibits textures described in sample KGK-1132/1 (figure 4a–h). Additionally, in sample KGK/1132/2, the majority of plagioclase feldspar grains have undergone conversion to antiperthite to varying degrees (see figure 5a). In these antiperthite grains, orthoclase rods are oriented in two different directions (figure 5b). Sometimes, plagioclase is converted to mesoperthite (figure 5c). Occasionally, only a portion of some matrix plagioclase grains were affected by the antiperthitization process (see figure 5d), but most experienced intense antiperthitization. Plagioclase and antiperthite frequently exhibit highly irregular grain boundaries, indicating amoeboid texture (figure 5e, f). Antiperthite grains with diffused grain boundaries are also present. These textural features suggest that antiperthitization in the sample is a result of the replacement of the original plagioclase rather than the exsolution of two feldspars during cooling after the peak metamorphism.

Formation of myrmekite is also prevalent at the grain boundaries of both plagioclase and antiperthite (see figure 5g, h, i) compared to sample KGK/1132/1. Occasionally, the entire grain margin of plagioclase is replaced by tiny quartz and orthoclase. In some microdomains, matrix orthoclase, plagioclase, and antiperthite are replaced by secondary calcite and sericite (see figure 5f). Matrix orthopyroxene (Opx_1) is frequently overprinted by biotite and chlorite. Locally, these biotites break down to produce fine-grain orthoclase + ilmenite ± rutile (occasionally pseudomorphing biotite. Tiny graphite and biotite-bearing microveins cross-cut the fractures of matrix mineral grains (figure 5j).

The majority of garnets broke down, producing vermicular orthopyroxene–plagioclase symplectite via reaction (2) (figure 5k), and later, these symplectites experienced intense alteration. Occasionally, these symplectites pseudomorph after garnets (figure 5k), similar to the sample KGK/1132/1 (figure 4h). Vermicular orthopyroxene grains are overprinted by biotite or chlorite. Plagioclase vermicules frequently dissolve. Secondary calcite formation can be identified at some of the outer margins of symplectites (figure 5l).

4.3 *Sample adjacent to a relatively thick vein (KGK/1132/3)*

This sample exhibits nearly all the textures documented in KGK/1132/2 (figure 5a–k). Additionally, several new mineralizations and replacement textures are present, primarily concentrated near the graphite veins. The intensity of mineral alteration is significantly higher in this sample compared to the previous two. Nearly all Opx_1 and Opx_2 are chloritized. Locally overprinted biotite also persists after the replacement of Opx_1 and Opx_2. In some domains, overprinted biotite has further altered to orthoclase + ilmenite ± rutile. Pl_1 grains experience dissolution along the grain boundaries (figure 6a, b, c). Pl_2 vermicules are also affected by significant

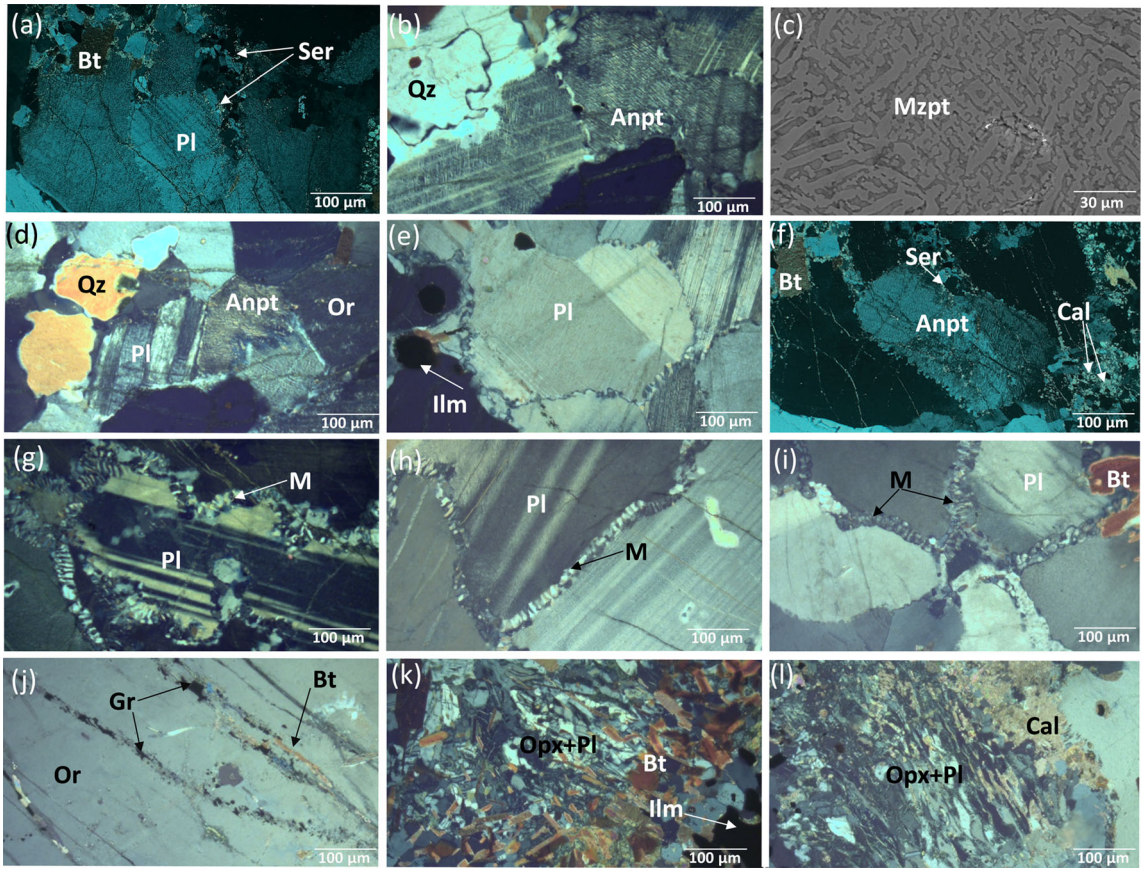

Figure 5. Petrography of sample KGK/1132/2. (**a**, **b**) Plagioclase feldspar grains have undergone conversion to antiperthite to varying degrees, (**c**) BSE image showing a mesoperthite, (**d**) a plagioclase grain (at the center of the figure) showing only half of the grain of plagioclase converted to antiperthite, (**e**, **f**) plagioclase and antiperthite frequently exhibit highly irregular grain boundaries, indicating amoeboid texture, (**g**, **h**, **i**) formation of myrmekite at the grain boundaries of both plagioclase and antiperthite, (**j**) tiny graphite and biotite-bearing microveins cross-cut the fractures of matrix mineral grains, (**k**) vermicular orthopyroxene–plagioclase symplectite in which orthopyroxene overprinted by biotite, (**l**) dissolved plagioclase vermicules in orthopyroxene + plagioclase symplectite. Secondary calcite formation can be identified at some of the outer margins of symplectites. Abbreviations are similar to figure 4. In addition, M – myrmekite.

dissolution. The formation of myrmekite after Pl_1 is dominant compared to sample KGK/1132/2 (figure 6d). Tiny veins (0.2–0.3 mm) of calcite extend from thin graphite veins toward the matrix (1–4 cm in length) of the host rock, following the fractures within the matrix minerals (see figure 6c). Occasionally, crystallized fine-grained quartz and orthoclase are present close to the graphite vein (figure 6e). Occasionally, disseminated biotite in the matrix breaks down to produce fine-grain orthoclase + ilmenite ± rutile ± siderite (occasionally pseudomorphic biotite, figure 6f).

4.4 *Mineralogy and textural features of rocks at contact zones and within graphite veins*

The percentages of graphite to gangue minerals in veins vary with the thickness of the veins. In tiny veins (0.3–1 cm in thickness), the graphite to gangue mineral percentages range from ∼80–95% graphite to 20–5% gangue minerals (see figure 7a, b, c). However, as the thickness of the vein increases, the intergrowth of gangue minerals with graphite drastically decreases.

At the contact between the host rock and graphite veins (abbreviated as CHGV), the crystallization of new mineral phases is prominent. Titanite is a mineral concentrated at CHGV, identified in three types of microdomains: (a) Xenomorphic fine-grained titanite (<0.1–0.25 cm) is present in domains where orthopyroxene–plagioclase (+ ilmenite) symplectite/moat pseudomorphs garnet (figure 7d). Occasionally, this titanite contains ilmenite inclusions. (b) Titanite occurs in chloritized matrix Opx_1-bearing domains (where the prominent mineral phases are chlorite,

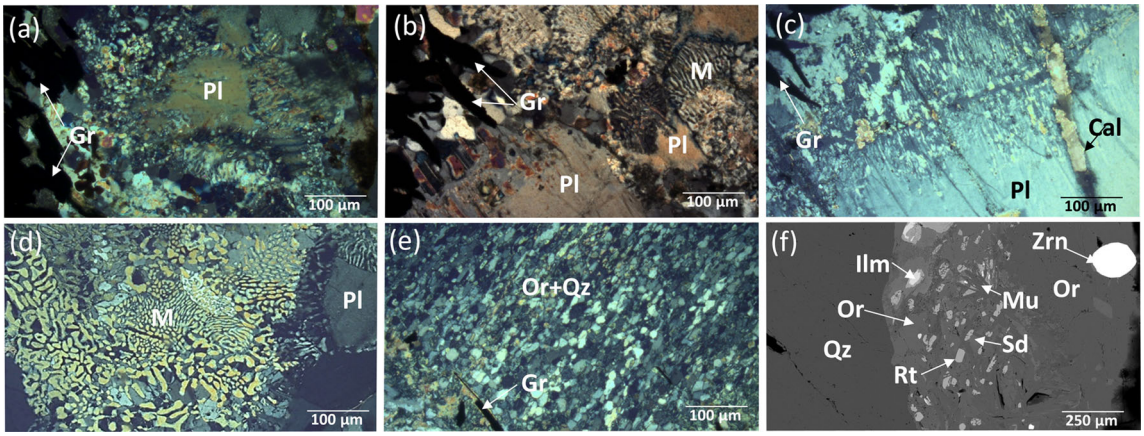

Figure 6. Petrography of sample KGK/1132/3. (**a**, **b**, **c**) Matrix plagioclase grains experience dissolution along the grain boundaries, (**d**) intense myrmekitization after matrix plagioclase, (**e**) crystallized fine-grained quartz and orthoclase are present close to the graphite vein, (**f**) biotite in the matrix breakdown to produce fine-grain orthoclase + ilmenite ± rutile ± siderite. Abbreviations are similar to figure 4. In addition: M – myrmekite, Sd – siderite, Ru – rutile, Zrn – zircon.

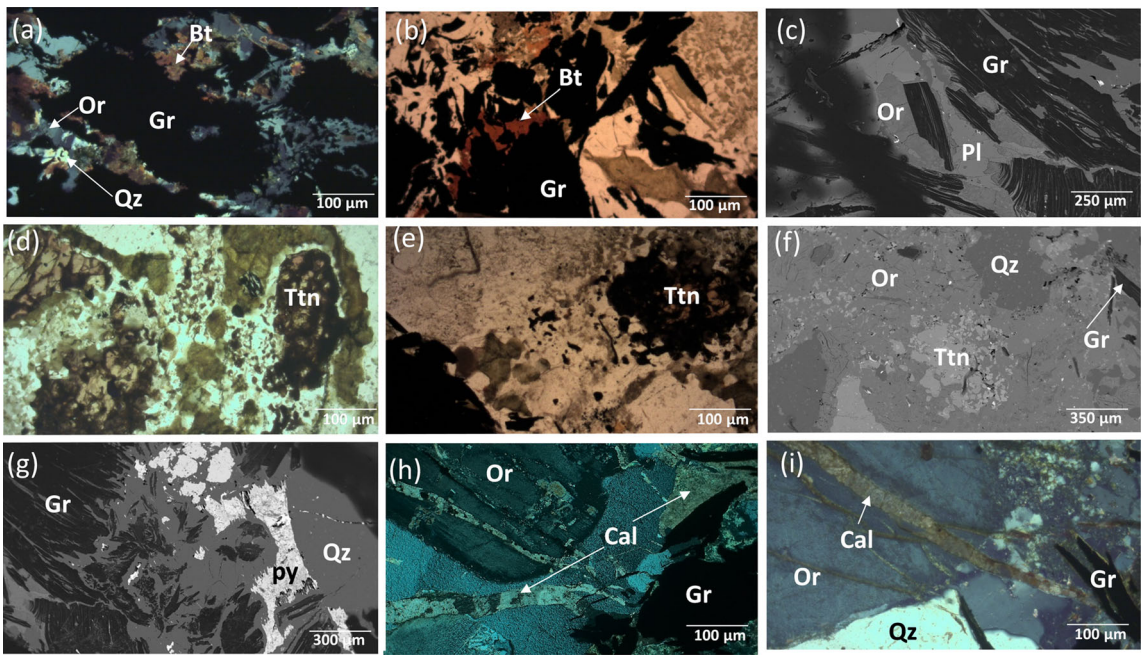

Figure 7. Petrography of graphite veins in the sample KGK/1132/3. (**a**, **b**, **c**) Occurrence of quartz, biotite feldspars among graphite flacks ((c) is a BSE image), (**d**) xenomorphic fine-grained titanite in domains where orthopyroxene–plagioclase moat. Orthopyroxene in highly chloritized, (**e**) titanite occurs in chloritized matrix orthopyroxene bearing domains, (**f**) titanites surrounded by precipitated quartz, plagioclase, and orthoclase, (**g**) occurrences of pyrite in graphite vein, (**h**, **i**) calcite veins are originated from graphite veins extend along the mineral fractures of the host rocks. Abbreviations are similar to figure 4. In addition, Ttn – titanite.

ilmenite, and crystallized plagioclase, figure 7e). (c) Rarely, titanites surrounded by precipitated quartz, plagioclase, and orthoclase are present (figure 7f). Clusters of monazites can also be identified in such domains.

Within the tiny graphite veins (0.3–0.75 cm in thickness), in addition to dominant graphite flakes (0.2–0.5 cm in length), xenomorphic quartz, plagioclase, orthoclase, and biotite are frequently present (figure 7a, b, c). Locally, xenomorphic pyrite (figure 7g) and calcite (figure 7h) are also present. Calcite veins originate from graphite veins that extend along the mineral fractures of the host rocks (figure 7i, j). In the central part of these tiny graphite veins, the majority of graphite flakes are oriented parallel to the direction of the vein. However, at the CHGV, the orientation of graphite flakes varies based on the mineralogy of the

host rock. Under the presence of medium to coarse-grained quartz, a sharp contact between graphite and quartz grains can be observed. Frequently, graphite flakes are oriented parallel to the grain margin of the quartz. In contrast, when the CHGV contains feldspars (primary or secondary), graphite flakes are arranged approximately perpendicular or oblique to the grain margins of the host rock.

4.5 *Characteristics of the wall rock (sample KGK/1132/4)*

The matrix of this garnet-bearing mafic granulite (wall rock) contains xenomorphic fine to medium-sized (0.2–0.5 cm) garnet, hypidiomorphic to xenomorphic plagioclase, alkali feldspar (<0.2 up to 0.5), xenomorphic orthopyroxene, and clinopyroxene as major minerals. Xenomorphic fine to medium-grain quartz and ilmenite are present as minor mineral phases. Apatite and biotite are the accessory constituents. Chlorite is the main secondary product. Additionally, the rock contains quartz and orthoclase feldspar-bearing melt ribs and nabs. Garnets are frequently broken down, forming corona textures via reaction (2). The outer margins of the corona mainly contain orthopyroxene–plagioclase motes, while the inner side of the corona contains orthopyroxene–plagioclase symplectites. At the CHGV in this sample, titanite, biotite, crystallized two feldspars, secondary calcite, and formation of myrmekite after plagioclase feldspar can be observed. Microcrystalline quartz, two feldspars, and biotite-bearing thin films (0.1 cm) are less parallel to the contact between the host rock and the graphite veins. Medium-grain titanite with ilmenite inclusions can be identified next to the immediate rock–vein contact.

5. Mineral chemistry

Mineral compositions were determined using JEOL JXA-8230 Field Emission Electron Probe Microanalyzers (EPMA) at the Centre for Earth Sciences, Indian Institute of Science, Bangalore, India. The analyses were conducted with an accelerating voltage of 15 kV, a beam current of 12 nA, and a spot size ranging from 1 to 3 μm. Mineral standards were utilized following the Astimex 53 Minerals Mount MINM25-53 protocol. The standards used were Na-albite-11.59, Fe-hematite-Fe^{3+}-99.68/Fe^{2+}-89.68, Mg-olivine-50.97, Si-quartz-100, Mn-rhodonite-42.3, Ti-rutile-100, K-orthoclase-15.57, Zn-willenite-64.68, Ca-diopside-24.8, Cr-chromium oxide-100, and for Al, Y-Al garnet-42.95. Data were calibrated using an oxide-ZAF correction program supplied by JEOL.

5.1 *Garnet*

Both Grt_1 and Grt_2 predominantly consist of almandine–pyrope solid solutions. Core and rim compositions of both Grt_1 indicate slight compositional zoning of Fe (table 1). The cores of Grt_1 and Grt_2 are slightly depleted in the almandine component, while the pyrope content shows the opposite behaviour to almandine. The grossular value of Grt_1 ($X_{Grs} \sim 0.15$) is slightly greater than that in Grt_2 ($X_{Grs} \sim 0.05$). Grt_1 contains a relatively high weight percent of MnO (MnO 1.9 wt%), compared to Grt_2 (MnO 0.5 wt%). The X_{Mg} of Grt_2 is slightly richer than Grt_1 (table 1).

5.2 *Biotite*

Biotite in the matrix of KGK/1132/1 and biotite in the tiny graphite veins, as well as overprinting after orthopyroxene in Opx–Pl symplectite in sample KGK/1132/3, are Mg-rich (X_{Mg} of ∼0.65, 0.8, and 0.8, respectively). Matrix biotite exhibits a relatively high TiO_2 content (up to 7 wt%) compared to the latter two types (5.6 and 6 wt%, respectively).

5.3 *Feldspars*

The matrix plagioclase (Pl_1) in KGK/1132/1 is albite-rich (Ab 0.60–0.65, table 1), while the matrix alkali feldspars are orthoclase-rich (Or up to 0.95, table 1). Alkali feldspar intergrown with graphite and crystallized alkali feldspars in the CHGV is also orthoclase-rich (Or 0.95, table 2). However, the total weight percentage of oxides in the latter orthoclase type is significantly low (up to 95.5 wt%) and indicates depletion of SiO_2 (up to 61.5%, table 2).

5.4 *Orthopyroxene*

The X_{Mg} value of unaltered matrix orthopyroxene (Opx_1) in KGK/1132/1 is ∼0.6 (table 1). The Al_2O_3 content is around 2.5 wt%. The X_{Al} value of

Table 1. *Representative EPMA data of minerals in sample KGK/1132/1.*

	Grt_1			Grt_2			Opx		Bt		Pl		Or		Ilm	
	Core	Mantle	Rim	Core	Mantle	Rim	Core	Rim	Core	Rim	Core	Rim	Core	Rim	In Grt_2	Matrix
SiO_2	38.62	38.61	38.35	39.39	39.23	38.73	51.99	52.21	37.91	38.15	59.89	59.98	65.06	65.23	0.00	0.03
TiO_2	0.07	0.12	0.03	0.08	0.03	0.14	0.09	0.06	7.01	6.46	0.07	bdl	0.04	0.06	52.88	52.51
Al_2O_3	21.49	21.50	21.54	22.02	22.25	21.47	2.43	2.58	13.98	14.01	25.50	25.93	18.86	18.79	0.04	0.03
Cr_2O_3	bdl	0.03	0.02	0.03	0.04	0.07	0.04	0.09	0.06	0.03	bdl	0.00	0.02	0.02	0.08	0.07
FeO	26.42	26.42	27.17	26.97	28.07	30.21	24.51	24.60	13.20	13.25	0.01	0.06	0.01	0.07	45.40	45.05
MnO	1.66	1.91	1.95	0.51	0.47	0.62	0.12	0.14	0.00	0.02	bdl	0.01	0.00	bdl	0.77	0.72
MgO	6.33	5.64	5.52	9.32	8.29	7.52	20.97	20.42	13.61	13.80	bdl	bdl	0.01	bdl	1.18	1.28
CaO	5.62	5.69	5.56	2.02	1.99	1.91	0.18	0.17	0.00	0.00	7.13	7.32	0.19	0.18	0.02	0.02
Na_2O	0.04	0.02	0.00	0.05	0.00	0.07	0.06	0.00	0.04	0.04	7.16	6.95	0.41	0.51	0.01	0.00
K_2O	0.01	0.01	0.00	0.00	0.03	0.02	0.01	0.00	10.31	10.11	0.20	0.20	15.79	15.50	0.00	0.00
ZnO	0.01	bdl	0.01	0.06	0.00	0.06	0.08	0.09	0.08	0.01	bdl	bdl	0.05	bdl	0.00	0.01
Total	**100.27**	**99.94**	**100.15**	**100.45**	**100.40**	**100.82**	**100.48**	**100.36**	**96.19**	**95.88**	**99.95**	**100.43**	**100.43**	**100.35**	**100.38**	**99.72**
O	12	12	12	12	12	12	6	6	22	22	8	8	8	8	3	3
Si	3.00	3.02	3.00	3.01	3.01	3.00	1.94	1.95	5.59	5.63	2.67	2.66	2.99	2.99	0.00	0.00
Ti	bdl	0.01	bdl	bdl	bdl	0.01	bdl	bdl	0.78	0.72	bdl	bdl	bdl	bdl	0.99	0.99
Al	1.97	1.98	1.99	1.98	2.01	1.96	0.11	0.11	2.43	2.44	1.34	1.35	1.02	1.02	0.00	0.00
Cr	bdl	bdl	bdl	0.00	0.00	0.00	bdl	bdl	0.01	0.00	bdl	bdl	bdl	bdl	0.00	0.00
Fe	1.72	1.73	1.78	1.72	1.80	1.96	0.77	0.77	1.63	1.64	bdl	bdl	bdl	bdl	0.95	0.95
Mn	0.11	0.13	0.13	0.03	0.03	0.04	bdl	bdl	bdl	bdl	bdl	bdl	bdl	bdl	0.02	0.02
Mg	0.73	0.66	0.64	1.06	0.95	0.87	1.17	1.14	2.99	3.04	bdl	bdl	bdl	bdl	0.04	0.05
Ca	0.47	0.48	0.47	0.17	0.16	0.16	0.01	0.01	bdl	bdl	0.34	0.35	0.01	0.01	0.00	0.00
Na	0.01	bdl	bdl	0.01	0.00	0.01	bdl	bdl	0.01	0.01	0.62	0.60	0.04	0.05	0.00	0.00
K	bdl	bdl	bdl	bdl	bdl	bdl	bdl	bdl	1.94	1.90	0.01	0.01	0.92	0.91	0.00	0.00
Zn	bdl	bdl	bdl	bdl	bdl	bdl	bdl	bdl	0.01	0.00	bdl	bdl	bdl	bdl	0.00	0.00
Total cation	**8.01**	**7.99**	**8.01**	**8.00**	**7.98**	**8.01**	**4.00**	**3.99**	**15.39**	**15.39**	**4.98**	**4.97**	**4.98**	**4.97**	**2.005**	**2.01**
Fe^{3+}	0.01	0.00	0.01	0.00	0.00	0.02	0.00	0.00								
Fe^{2+}	1.71	1.73	1.77	1.73	1.80	1.94	0.76	0.77								
Alm	0.57	0.58	0.59	0.58	0.61	0.65										
Spe	0.04	0.04	0.04	0.01	0.01	0.01										
Pyr	0.24	0.22	0.21	0.36	0.32	0.29										
Grs	0.15	0.16	0.15	0.05	0.07	0.04										

Table 1. *(Continued.)*

	Grt_1			Grt_2		Opx		Bt	Pl		Or		Ilm	
	Core	Mantle	Rim	Core	Mantle	Rim	Core	Rim	Core	Rim	Core	Rim	In Grt_2	Matrix
Fs							0.39	0.40						
En							0.60	0.59						
Wo							0.00	0.00	0.35	0.36	0.01	0.01		
An									0.64	0.62	0.04	0.05		
Ab									0.01	0.01	0.95	0.94		
Or														
X_{Mg}	0.30	0.28	0.27	0.38	0.34	0.31	0.60	0.60	0.65	0.65				

bdl: Below the detection limit.

Opx_1 is ∼0.06 (table 1). Due to extreme alteration, the composition of symplectitic orthopyroxene after garnet (Opx_2) could not be measured, and only pseudomorphic shapes of vermicular orthopyroxene have been preserved.

5.5 *Titanite*

The total oxide weight present in titanite is close to 97.75, indicating the possible incorporation of some metallic elements (table 2). Titanite contains Al_2O_3 up to 1.5 wt%.

6. Discussion

6.1 *Wall rock alteration due to graphite mineralization*

The petrographic evidence from this study reveals a progressive increase in wall rock alteration towards the graphite vein. Antiperthitization (figure 5b, d) and myrmekite formation (figure 5g, h, i) are prominent alteration features, with both intensifying from the host rock to the vein, indicating their link to hydrothermal alteration processes. Similar findings have been reported by Kehelpannala (1995, 1999) and Touret *et al.* (2019) in the Kahatagaha and Bogala mines in Sri Lanka. The following sections explore the mechanisms that contributed to the antiperthitization and myrmekite observed in the samples studied.

Yuguchi and Nishiyama (2008) have emphasized the involvement of exchange cycles in the formation of myrmekite and reaction rims, elucidating a fundamental mechanism rooted in the albitization of plagioclase facilitated by the diffusive transport of $NaO_{1/2}$ and SiO_2 (4):

$$CaAl_2Si_2O_8 + NaO_{1/2} + SiO_2 = NaAlSi_3O_8 + CaO + AlO_{3/2}. \quad (4)$$

The formation of myrmekite necessitates higher SiO_2 content than reaction rim development. Some SiO_2 comes from plagioclase decomposition (figure 5e–h), while the surrounding environment contributes to the plagioclase boundary (Yuguchi and Nishiyama 2008). Simpson and Wintsch (1989) observed enhanced myrmekite growth in deformed rocks under high normal stress on feldspar, attributing strain energy as the driving force. Models for antiperthite formation occur concurrently with those for myrmekite (Song *et al.* 2024), suggesting mechanisms such as

Table 2. *Representative EPMA data of minerals in sample KGK/1132/3.*

	Bt*		Bt**										
Mineral	Core	Rim	Core	Rim	Tit*	Tit**	Or*	Or**	Ilm*	Qz*	Cal**	Sd**	Py*
SiO_2	37.91	37.82	37.71	37.17	30.15	30.25	61.34	61.54	0.67	99.62	0.13	bdl	0.36
TiO_2	5.52	5.41	5.76	6.18	37.34	37.27	0.00	0.12	52.87	0.05	0.00	bdl	bdl
Al_2O_3	13.12	13.24	13.47	13.42	1.60	1.45	18.77	18.55	0.06	0.06	0.11	0.04	0.08
Cr_2O_3	0.11	0.15	0.19	0.19	0.13	0.11	bdl	bdl	0.23	0.02	bdl	0.01	bdl
FeO	15.87	15.36	15.31	16.06	0.70	0.57	0.21	0.36	44.71	0.11	0.21	14.38	40.25
MnO	0.06	0.06	0.09	0.04	0.14	0.10	0.04	0.00	1.30	0.03	0.52	0.19	bdl
MgO	12.45	12.46	12.59	12.03	0.07	0.10	0.04	0.06	0.50	0.05	0.18	11.28	0.02
CaO	0.12	0.11	0.11	0.05	27.50	27.88	0.10	0.06	bdl	0.08	56.04	26.81	0.01
Na_2O	0.07	0.04	0.03	0.02	0.01	0.00	0.40	0.43	bdl	bdl	bdl	0.02	0.15
K_2O	9.79	9.61	9.68	9.64	0.00	0.00	14.09	14.27	bdl	bdl	0.26	0.04	bdl
ZnO	bdl	0.09	0.08	0.18	0.01	0.00	0.05	bdl	bdl	bdl	0.48	0.11	bdl
CO_2											42.07	47.13	
Total	**95.03**	**94.33**	**95.01**	**95.01**	**97.65**	**97.73**	**95.04**	**95.39**	**100.37**	**100.01**	**100.0**	**100.00**	**40.87**
O	22.00	22.00	22.00	22.00	22.00	22.00	8.00	8.00	3.00	2.00	2.00	2.00	
Si	5.72	5.73	5.68	5.63	4.43	4.44	2.96	2.97	0.02	1.00	bdl	bdl	
Ti	0.63	0.62	0.65	0.70	4.13	4.11	bdl	bdl	0.99	bdl	bdl	bdl	
Al	2.33	2.36	2.39	2.39	0.28	0.25	1.07	1.05	bdl	bdl	bdl	bdl	
Cr	0.01	0.02	0.02	0.02	0.01	0.01	bdl	bdl	bdl	bdl	bdl	bdl	
Fe	2.00	1.95	1.93	2.03	0.09	0.07	0.01	0.01	0.93	bdl	0.46	0.42	
Mn	0.01	0.01	0.01	0.01	0.02	0.01	bdl	bdl	0.03	bdl	0.01	0.01	
Mg	2.80	2.81	2.82	2.71	0.02	0.02	bdl	bdl	0.02	bdl	0.54	0.58	
Ca	0.02	0.02	0.02	0.01	4.33	4.39	0.01	bdl	bdl	bdl	0.95	0.99	
Na	0.02	0.01	0.01	0.01	bdl	bdl	0.04	0.04	bdl	bdl	bdl	bdl	
K	1.89	1.86	1.86	1.86	bdl	bdl	0.87	0.88	bdl	bdl	bdl	bdl	
Zn	bdl	0.01	0.01	0.02	bdl	bdl	0.00	bdl	bdl	bdl	bdl	bdl	
Total cation	**15.43**	**15.39**	**15.40**	**15.40**	**13.30**	**13.31**	4.96	**4.96**	**1.99**	**1.00**	**1.96**	**2.01**	
Fe^{3+}	1.19	1.14	1.14	1.15									
Fe^{2+}	0.81	0.81	0.78	0.88									
X_{Mg}	0.77	0.78	0.78	0.75									
An							0.01	0.00					
Ab							0.04	0.04					
Or							0.95	0.95					

* Minerals within tiny graphite vein. ** Minerals within the contact zone of the host rock with graphite vein.

metasomatic replacement of plagioclase by alkali feldspar in slowly cooled granulite-facies rocks (Sen 1959), simultaneous crystallization (Vogel 1970), and exsolution from ternary feldspar (Kay 1977). The increasing antiperthitization from the host rock to the graphite vein in this study (figures 4, 5, and 6) indicates metasomatic replacement as the key mechanism. Kehelpannala (1995) noted that alkali metasomatism forms alteration zones around graphite veins, transforming plagioclase to antiperthite and then to sericite. Crystallization of alkali feldspar in potassium-poor plagioclase likely occurs via heterogeneous nucleation on plagioclase interfaces due to low activation energy (Vogel 1970).

Feldspar dissolution has been identified as a potential mechanism for facilitating CO_2 sequestration through several processes, including the consumption of hydrogen ions (H^+), generation of bicarbonate ions (HCO_3^-), and buffering of pH in formation water (Giles and Marshall 1986; Emery *et al.* 1990; França *et al.* 2003; Bjørlykke and Jahren 2012; Yuan *et al.* 2019). When CO_2 dissolves in water-bearing fluids, it forms carbonic acid, releasing H^+ ions that catalyze feldspar dissolution reactions (Giles and Marshall 1986; Emery *et al.* 1990; França *et al.* 2003; Bjørlykke and Jahren 2012).

The dissolution of feldspar in the host rock is commonly observed towards the graphite vein (figure 6) and plays a significant role in the long-term fate of injected CO_2. This dissolution not only consumes acidity but also produces alkalinity, increasing the saturation index of carbonate phases and potentially leading to the permanent storage of CO_2 in carbonate minerals (Bickle 2009; Wigley

et al. 2013). The precipitation of secondary minerals, such as calcite, following feldspar dissolution further enhances CO_2 capture (Yuan *et al.* 2019). Specifically, the formation of secondary calcite (figures 2e, 6h) in altered wall rock results from the combination of Ca^{2+} from plagioclase dissolution and CO_3^{2-} from CO_2.

The crystallization of two feldspar varieties at the CHGV also indicates the products of wall rock alteration (figure 5a, b, e). Key elements – Ca, Na, K, Al, and Si – likely originate from feldspar dissolution and antiperthitization during this alteration process, with additional silica contributions from hydrothermal fluids responsible for graphite mineralization. The presence of vein quartz within graphite veins in this study (figure 2d), also as reported by Kehelpannala (1995, 1999) and Touret *et al.* (2019), supports the role of Si in hydrothermal fluids during graphite precipitation. Furthermore, the dissolution–reprecipitation mechanisms of feldspar have been thoroughly examined in various studies (Hellmann *et al.* 2003, 2012, 2015; Ruizggudo *et al.* 2012, 2016; Putnis 2014).

Biotite crystallization at the CHGV (figure 6a, b) and its overprint on symplectitic orthopyroxene (figures 4h, 5k) indicate the role of H_2O during wall rock alteration. Elements like K and Al likely originate from antiperthitic plagioclase (figure 5b, d) and feldspar dissolution (figure 6a, b, c), while Si may come from feldspar alteration and hydrothermal fluid activity. Fe in biotite may have been sourced from orthopyroxene (figures 4h, 5k) or the hydrothermal fluid, as supported by the presence of pyrite in Sri Lankan vein graphite (Kehelpannala 1995, 1999; Touret *et al.* 2019) (figure 2f), suggesting Fe as a component of the fluid.

H_2O could originate from two potential sources: pre-existing retrograde H_2O-saturated fluids/melts within the host rock, possibly from prograde dehydration (Touret and Huizenga 2012; Huizenga *et al.* 2014; Dharmapriya *et al.* 2015a, b), or from the mineralization of vein graphite. Retrograde biotite formation provides evidence for H_2O-rich fluids during retrogression, which facilitated symplectitic textures (White *et al.* 2007).

Regarding vein graphite formation, fluid cooling (Huizenga 2011; Luque *et al.* 2014), rather than fluid–fluid mixing, likely led to graphite precipitation (Touret *et al.* 2019). CO_2 reduction, driven by redox contrast between CO_2 fluid and the host rock, likely facilitated graphite formation (Touret and Huizenga 2012), as shown in the reaction:

$$CO_2 \rightarrow C + O_2. \quad (5)$$

This process, occurring under granulite facies conditions, was likely key during near-isothermal decompression. The association of pyrite and graphite (Katz 1987) suggests that pyrrhotite may have acted as a reducing agent, contributing to early graphite and pyrite formation under high-temperature conditions (Kirilova *et al.* 2018a, b).

Touret *et al.* (2019) proposed that during cooling, the graphite precipitation reaction (6), as described by Huizenga (2011), occurs:

$$CO_2 + 2H_2 \rightarrow C + 2H_2O. \quad (6)$$

The H_2O produced could support biotite formation during wall rock alteration. Consuming H_2O in hydrous mineral formation may drive further graphite precipitation, similar to the Borrowdale graphite deposit in the UK (Ortega *et al.* 2010).

Titanite, primarily associated with ilmenite at CHGV (figure 6d, e, f), suggests that Ti comes from ilmenite, while Ca is derived from plagioclase alteration. Si contributions likely come from feldspar alteration and hydrothermal fluids. Kehelpannala (1995, 1999) noted the absence of primary graphite in the host rock, but this study reveals disseminated graphite associated with the veins. This indicates hydrothermal fluid infiltration along grain boundaries and fractures, supported by plagioclase alteration (figure 6a, b, c) and calcite precipitation in fractures (figure 6h, i). Decompression-induced grain fracturing, as discussed by Hiroi *et al.* (2014), further supports this interpretation.

Earlier studies found higher gangue mineral concentrations in smaller graphite veins, decreasing towards the center of thicker veins (Silva 1987; Dissanayake *et al.* 1988; Kehelpannala 1999; Touzain *et al.* 2010). Gangue minerals mechanically adhere to graphite surfaces or are intercalated between graphene layers (Touzain *et al.* 2010). Chemical analysis of these deposits reveals trace elements like Fe, Ca, Mg, Si, Al, and Na, along with lower concentrations of transition metals such as Cu, Ni, Co, and Zn (Dissanayake *et al.* 1988).

Based on petrographic observations in this study (figures 4, 5, 6), feldspar dissolution likely contributes to a slightly acidic environment by consuming hydrogen ions (H^+), generating bicarbonate ions (HCO_3^-), and buffering the pH of formation water (Yuan *et al.* 2019). This process adds Ca, Na, K, and Si to the CO_2-rich

hydrothermal fluid, potentially facilitating the formation of antiperthite and myrmekite. Additionally, Fe, Ca, Mg, Si, Al, and Na likely originate from the alteration of host rock minerals, including feldspar, biotite, and pyroxene, during wall rock alteration. Silicon may also be present in the hydrothermal fluid, as evidenced by large vein quartz formations within graphite veins (Touret *et al.* 2019). Moreover, the occurrence of trace metals such as Cu, Ni, Co, and Zn in hydrothermal fluids has been well-documented in various mineral deposits worldwide (Liu *et al.* 2011, 2012; Migdisov *et al.* 2011; Tian *et al.* 2012; Jonsson and Liu 2020).

6.2 *Implications for the relative timing of vein graphite mineralization in Sri Lanka*

The petrographic evidence presented herein facilitates the determination of the relative age of vein graphite mineralization in Sri Lanka. Several researchers have proposed a clockwise P–T trajectory for the rocks in the Highland Complex (HC) and Western Complex (WC) (Hiroi *et al.* 1994; Raase and Schenk 1994; Dharmapriya *et al.* 2014, 2015a, b, 2017b; Hirayama *et al.* 2020). These studies suggest that after reaching peak metamorphic conditions, both HC and WC rocks experienced a period of near isobaric cooling (IBC) as evidenced by the formation of fine-grained granules (Perera 1987; Prame 1991; Schumacher *et al.* 1990; Mathavan and Fernando 2001; Dharmapriya *et al.* 2014, 2015a, b). Subsequently, the rocks underwent a near-isothermal decompression stage (ITD) (Perera 1987; Sandiford *et al.* 1988; Schumacher *et al.* 1990; Prame 1991; Dharmapriya *et al.* 2015b, 2021a, b).

The graphite veins observed cutting across gneissic foliations of granulite-facies rocks in the Kahatagaha mine indicate their retrograde origin (Kehelpannala 1999). Furthermore, these graphite veins intersect the axial planes of large-scale synforms and antiforms, providing solid evidence for the origin of graphite veins postdating the major folding event of the Sri Lankan basement (Kehelpannala 1999; Touret *et al.* 2019).

Thermobarometric calculations on rocks from the HC revealed that the isothermal decompression corresponded to temperatures ∼750–830°C and pressures ranging from 6.5 to 5 kbar (Schenk *et al.* 1991; Hiroi *et al.* 1994; Kleinschrodt 1994; Raase and Schenk 1994). Dharmapriya *et al.* (2014) also noted that in the southwestern part of the HC, close to the inferred HC–WC boundary, the rocks experienced post-peak evolution characterized by a stage of nearly isobaric cooling down to T of 770°C and P of 7.5 kbar, followed by a late stage of isothermal decompression down to $P < 6.5$ kbar and T of 770°C. These conditions are indicative of granulite facies metamorphism, as evidenced by orthopyroxene-bearing symplectites. Alterations observed in both orthopyroxene and plagioclase near the graphite veins, produced during decompression, indicate that vein graphite formation occurred during or after the decompression stage (Kehelpannala 1995). Similar observations were made by Kehelpannala (1995) in the same mine. However, the absolute timing of this decompression stage has yet to be established by geochronological studies. New minerals frequently form by overprinting existing minerals during the retrogression of high-grade metamorphic rocks (e.g., Brown 2002; Ouzegane *et al.* 2003; Beach and Tarney 1978; Zhang *et al.* 2020). The generation of minerals and assemblages during retrograde metamorphism has been reported in both the HC and WC of Sri Lanka by several authors, with biotite being one of the common retrograde minerals (e.g., Hiroi *et al.* 1994; Raase and Schenk 1994; Dharmapriya *et al.* 2014, 2017a, b, 2021a, b). However, in the studied samples, the tiny biotite flakes in the CHGV indicate that their formation occurred simultaneously with the mineralization of vein graphite. Some of the biotite intergrown with graphite flakes clearly supports this interpretation (figure 7a, b). The alteration of orthopyroxene in the Opx–Pl symplectite after garnet (figure 4h), occurring only near the CHGV, also indicates a direct influence of the hydrothermal fluid responsible for graphite mineralization on the aforementioned alteration. Meanwhile, the mineral chemistry of overgrowth biotite after orthopyroxene in these symplectites and biotite intergrown with graphite at the CHGV shows similar mineral chemistry (table 2), indicating their cogenesis.

7. Conclusions

The detailed analysis of wall rock alteration and graphite mineralization in the Kahatagaha–Kolongaha sheds light on the complex geological processes governing vein graphite formation. The petrographic examination has uncovered a progressive increase in alteration in wall rock towards graphite veins. This included the formation of antiperthite and myrmekite, alteration of orthopyroxene, dissolution of plagioclase,

and the crystallization of new minerals, such as two feldspar varieties, biotite, and titanite, indicative of hydrothermal alteration processes. The existence of slightly acidic conditions, attributed to the interaction of CO_2 and H_2O, facilitates the dissolution of feldspar in the host rock, contributing to the derivation of Ca, Na, K, Si, and Al, serving as potential sources for antiperthitization and myrmekite formation. Overall, wall rock alterations suggest the combined contribution of both host rock minerals and hydrothermal fluids to the formation of alteration products such as biotite, titanite, two feldspars, and calcite.

Our findings support previous research indicating that these graphite veins formed after major tectonic events, such as large-scale folding, during a period of retrograde metamorphism. This study emphasizes the critical role of fluid-rock interaction in the genesis of vein graphite. Revealing these processes is essential for guiding future exploration and development efforts targeting such economically valuable mineral resources.

Acknowledgements

This research received support from the National Research Council of Sri Lanka under Grant No. 15-007, Grant No. 19-092, and the PGIS Research Grant No. 2020/18. We extend our sincere gratitude to two anonymous reviewers for their valuable contributions in providing volume corrections, insightful comments, and suggestions that helped to improve the original version of this manuscript. We also kindly acknowledge Dr George Mathew for his careful handling of our manuscript and for offering invaluable comments that have significantly enhanced its quality.

Author statement

T C Senevirathna: Sample collection (supporting), sample preparation for analysis (lead), formal analysis (supporting), data interpretation (supporting), writing – original draft (supporting). P L Dharmapriya: Conceptualization (supporting), sample collection (supporting), methodology (lead), sample preparation for analysis (supporting), sample analysis (lead), data interpretation (lead), writing – original draft (lead), writing – review and editing (lead). N W B Balasooriya: Conceptualization (supporting), sample collection (lead), methodology (supporting), formal analysis (supporting), data interpretation (supporting), writing – original draft (supporting), writing – review and editing (supporting), supervision (lead). H M T G A Pitawala: Conceptualization (lead), methodology (supporting), writing – original draft (supporting), writing – review and editing (supporting), supervision (lead). H W M A C Wijayasinghe: Project administration (lead), methodology (supporting), supervision (lead), writing – original draft (supporting), writing – review and editing (supporting). Medhavi Abeysinghe: Formal analysis (supporting). K Sajeev: Formal analysis (supporting), writing – original draft (supporting), writing – review and editing (supporting).

References

Almond D C 1991 Arena Gneiss and Kandy Gneiss – A proposed subdivision of the Highland Series around Kandy, and its significance; *J. Geol. Soc. Sri Lanka* **3** 41–50.

Balasooriya N W B, Dahanayake K, Touzain P and Bandaranayake P W S K 2002 Structure characteristics of Sri Lanka graphite; *Ceylon J. Sci. (Phys. Sci.)* **9(2)** 41–48.

Barnes H L (ed.) 1997 *Geochemistry of hydrothermal ore deposits*; John Wiley & Sons.

Beach A and Tarney J 1978 Major and trace element patterns established during retrogressive metamorphism of granulite-facies gneisses, NW Scotland; *Precamb. Res.* **7(4)** 325–348, https://doi.org/10.1016/0301-9268(78)90046-3.

Berger A R and Jayasinghe N R 1976 Precambrian structure and chronology in the Highland Series of Sri Lanka; *Precamb. Res.* **3(6)** 559–576, https://doi.org/10.1016/0301-9268(76)90019-X.

Bhattacharya A, Krishnakumar K R, Raith M and Sen S K 1991 An improved set off a-X parameters for Fe-Mg-Ca garnets and refinements of the orthopyroxene-garnet thermometer and the orthopyroxene-garnet-plagioclase-quartz barometer; *J. Petrol.* **32(3)** 629–656, https://doi.org/10.1093/petrology/32.3.629.

Bickle M J 2009 Geological carbon storage; *Nat. Geosci.* **2(12)** 815–818, https://doi.org/10.1038/ngeo687.

Binu-Lal S S, Kehelpannala K W, Satish-Kumar M and Wada H 2003 Multistage graphite precipitation through protracted fluid flow in sheared metagranitoid, Digana, Sri Lanka: Evidence from stable isotopes; *Chem. Geol.* **197(1–4)** 253–270, https://doi.org/10.1016/S0009-2541(02)00400-X.

Bjørlykke K and Jahren J 2012 Open or closed geochemical systems during diagenesis in sedimentary basins: Constraints on mass transfer during diagenesis and the prediction of porosity in sandstone and carbonate reservoirs; *AAPG Bull.* **96(12)** 2193–2214, https://doi.org/10.1306/04301211139.

Brown M 2002 Retrograde processes in migmatites and granulites revisited; *Metamorph. Geol.* **20(1)** 25–40, https://doi.org/10.1046/j.0263-4929.2001.00362.x.

Cooray P G 1984 An introduction to the geology of Ceylon; *Natl. Mus. Ceylon* **31(1)** 324, https://doi.org/10.1017/S0016756800018148.

Cooray P G 1994 The Precambrian of Sri Lanka: A historical review; *Precamb. Res.* **66(1–4)** 3–18, https://doi.org/10.1016/0301-9268(94)90041-8.

Dharmapriya P L, Malaviarachchi S P, Galli A, Su B X, Subasinghe N D, Dissanayake C B, Nimalsiri T B and Zhu B 2014 P–T evolution of a spinel + quartz bearing khondalite from the Highland Complex, Sri Lanka: Implications for non-UHT metamorphism; *J. Asian Earth Sci.* **95** 99–113, https://doi.org/10.1016/j.jseaes.2014.05.003.

Dharmapriya P L, Malaviarachchi S P, Galli A, Su B X, Subasinghe N D and Dissanayake C B 2015a Rare evidence for formation of garnet + corundum during isobaric cooling of ultrahigh temperature metapelites: New insights for retrograde P–T trajectory of the Highland Complex, Sri Lanka; *Lithos* **220** 300–317, https://doi.org/10.1016/j.lithos.2015.01.015.

Dharmapriya P L, Malaviarachchi S P, Santosh M, Tang L and Sajeev K 2015b Late-neoproterozoic ultrahigh-temperature metamorphism in the Highland Complex, Sri Lanka; *Precamb. Res.* **271** 311–333, https://doi.org/10.1016/j.precamres.2015.10.010.

Dharmapriya P L, Malaviarachchi S P, Kriegsman L M, Galli A, Osanai Y, Subasinghe N D and Dissanayake C B 2017a Distinct metamorphic evolution of alternating silica-saturated and silica-deficient microdomains within garnet in ultrahigh-temperature granulites: An example from Sri Lanka; *Geosci. Front.* **8(5)** 1115–1133, https://doi.org/10.1016/j.gsf.2016.11.008.

Dharmapriya P L, Malaviarachchi S P, Kriegsman L M, Galli A, Sajeev K and Zhang C 2017b New constraints on the P–T path of HT/UHT metapelites from the Highland Complex of Sri Lanka; *Geosci. Front.* **8(6)** 1405–1430, https://doi.org/10.1016/j.gsf.2016.12.005.

Dharmapriya P L, Malaviarachchi S P, Kriegsman L M, Galli A, Dyck B, Sajeev K, Su B X and Pitawala A 2020 Symplectite growth in the presence of alkaline fluids: Evidence from high-aluminous metasediments of the Highland Complex, Sri Lanka; *Miner. Petrol.* **114** 515–538, https://doi.org/10.1007/s00710-020-00710-2.

Dharmapriya P L, Malaviarachchi S P, Galli A, Kriegsman L M, Osanai Y, Sajeev K, Su B X, Tsunogae T, Zhang C, Adachi T and Dissanayake C B 2021a Hybrid phase equilibria modelling with conventional and trace element thermobarometry to assess the P–T evolution of UHT granulites: An example from the Highland Complex, Sri Lanka; *J. Metamorph. Geol.* **39(2)** 209–246.

Dharmapriya P L, Kriegsman L and Malaviarachchi S P 2021b Spatial distribution of ultrahigh-temperature granulites of the Highland Complex of Sri Lanka: Lowermost continental crust above an ultrahot palaeo-Moho; *Lithos* **404–405** 1–11, https://doi.org/10.1016/j.lithos.2021.106484.

Ding X, Harlov D E, Chen B and Sun W 2018 Fluids, metals, and mineral/ore deposits; *Geofluids* **2018** 1–6, https://doi.org/10.1155/2018/1452409.

Dissanayake C B 1994 Origin of vein graphite in high-grade metamorphic terrains: Role of organic matter and sediment subduction; *Miner. Deposita* **29** 57–67, https://doi.org/10.1007/BF03326396.

Dissanayake C B, Gunawardena R P and Dinalankara D M S K 1988 Trace elements in vein graphite of Sri Lanka; *Chem. Geol.* **68(1–2)** 121–128, https://doi.org/10.1016/0009-2541(88)90091-5.

Dobner A, Graf W, Hahn-Weinheimer P and Hirner A 1978 Stable carbon isotopes of graphite from Bogala Mine, Sri Lanka; *Lithos* **11(3)** 251–255, https://doi.org/10.1016/0024-4937(78)90025-7.

Emery D, Myers K J and Young R 1990 Ancient subaerial exposure and freshwater leaching in sandstones; *Geology* **18(12)** 1178–1181, https://doi.org/10.1130/0091-7613(1990)018%3C1178:ASEAFL%3E2.3.CO;2.

Erdosh G 1970 Geology of Bogala Mine, Ceylon and the origin of vein-type graphite; *Miner. Deposita* **5** 375–382, https://doi.org/10.1007/BF00206734.

Fernando G W A R, Hauzenberger C A, Baumgartner L P and Hofmeister W 2003 Modeling of retrograde diffusion zoning in garnet: Evidence for slow cooling of granulites from the Highland Complex of Sri Lanka; *Miner. Petrol.* **78** 53–71, https://doi.org/10.1007/s00710-002-0224-1.

França A B, Araújo L M, Maynard J B and Potter P E 2003 Secondary porosity formed by deep meteoric leaching: Botucatu eolianite, southern South America; *AAPG Bull.* **87(7)** 1073–1082, https://doi.org/10.1306/02260301071.

Ganguly J, Cheng W and Tirone M 1996 Thermodynamics of aluminosilicate garnet solid solution: New experimental data, an optimized model, and thermometric applications; *Contrib. Mineral. Petrol.* **126** 137–151, https://doi.org/10.1007/s004100050240.

Giles M R and Marshall J D 1986 Constraints on the development of secondary porosity in the subsurface: Re-evaluation of processes; *Mar. Petrol. Geol.* **3(3)** 243–255, https://doi.org/10.1016/0264-8172(86)90048-6.

Hapuarachchi D J A C 1977 Decarbonation reactions and the origin of vein-graphite in Sri Lanka; *J. Natn. Sci. Coun. Sri Lanka* **5(1)** 29–32.

He X F, Santosh M, Tsunogae T and Malaviarachchi S P 2016 Early to late Neoproterozoic magmatism and magma mixing-mingling in Sri Lanka: Implications for convergent margin processes during Gondwana assembly; *Gondwana Res.* **32** 151–180, https://doi.org/10.1016/j.gr.2015.02.013.

Hellmann R, Penisson J M, Hervig R L, Thomassin J H and Abrioux M F 2003 An EFTEM/HRTEM high-resolution study of the near surface of labradorite feldspar altered at acid pH: Evidence for interfacial dissolution-reprecipitation; *Phys. Chem. Miner.* **30** 192–197, https://doi.org/10.1007/s00269-003-0308-4.

Hellmann R, Wirth R, Daval D, Barnes J P, Penisson J M, Tisserand D, Epicier T, Florin B and Hervig R L 2012 Unifying natural and laboratory chemical weathering with interfacial dissolution-reprecipitation: A study based on the nanometer-scale chemistry of fluid-silicate interfaces; *Chem. Geol.* **294** 203–216, https://doi.org/10.1016/j.chemgeo.2011.12.002.

Hellmann R, Cotte S, Cadel E, Malladi S, Karlsson L S, Lozano-Perez S, Cabié M and Seyeux A 2015 Nanometer-scale evidence for interfacial dissolution-reprecipitation control of silicate glass corrosion; *Nat. Mater.* **14(3)** 307–311, https://doi.org/10.1038/nmat4172.

Henry D J, Guidotti C V and Thomson J A 2005 The Ti-saturation surface for low-to-medium pressure metapelitic biotites: Implications for geothermometry and Ti substitution mechanisms; *Am. Mineral.* **90(2–3)** 316–328, https://doi.org/10.2138/am.2005.1498.

Hewathilake H P T S, Balasooriya N W B, Pitawala H M T G A and Wijayasinghe H W M A C 2015 Use of crystal

morphologies to unravel the origin of vein graphite in Sri Lanka; *J. Geol. Soc. Sri Lanka* **17** 65–73.

Hewathilake H P T S, Balasooriya N W B, Nakamura Y, Pitawala H M T G A, Wijayasinghe H W M A C and Satish-Kumar M 2018 Geochemical, structural and morphological characterization of vein graphite deposits of Sri Lanka: Witness to carbon rich fluid activity; *J. Miner. Petrol. Sci.* **113(2)** 96–105, https://doi.org/10.2465/jmps.170721.

Hirayama E, Tsunogae T, Malaviarachchi S P, Takamura Y, Dharmapriya P L and Tsutsumi Y 2020 Prolonged Neoproterozoic high-grade metamorphism of the Wanni Complex, Sri Lanka: New insights from petrology, phase equilibria modelling, and zircon U–Pb geochronology of partially melted cordierite gneiss from Walpita; *Geol. J.* **55(9)** 6147–6168, https://doi.org/10.1002/gj.3792.

Hiroi Y, Ogo Y and Namba K 1994 Evidence for prograde metamorphic evolution of Sri Lankan pelitic granulites, and implications for the development of continental crust; *Precamb. Res.* **66(1–4)** 245–263, https://doi.org/10.1016/0301-9268(94)90053-1.

Hiroi Y, Yanagi A, Kato M, Kobayashi T, Prame B, Hokada T, Satish-Kumar M, Ishikawa M, Adachi T, Osanai Y and Motoyoshi Y 2014 Supercooled melt inclusions in lower-crustal granulites as a consequence of rapid exhumation by channel flow; *Gondwana Res.* **25(1)** 226–234, https://doi.org/10.1016/j.gr.2013.04.001.

Hölzel S, Köhler H, Kröner A, Jaeckel P and Liew T C 1991 Geochronology of the Sri Lankan Basement; In: *The Crystalline Crust of Sri Lanka, Part I. Summary of Research of the German-Sri Lankan Consortium* (ed.) Kröner A, Geological Survey Department Sri Lanka, Professional Papers **5** 236–257.

Hölzel S, Hofmann A W, Todt W and Köhler H 1994 U and Pb geochronology of the Sri Lankan basement; *Precamb. Res.* **66(1–4)** 123–149, https://doi.org/10.1016/0301-9268(94)90048-5.

Huizenga J M 2011 Thermodynamic modelling of a cooling C-O-H fluid-graphite system: Implications for hydrothermal graphite precipitation; *Miner. Deposita* **46** 23–33, https://doi.org/10.1007/s00126-010-0310-y.

Huizenga J M, van Reenen D and Touret J L R 2014 Fluid-rock interaction in retrograde granulites of the Southern Marginal Zone, Limpopo high grade terrain, South Africa; *Geosci. Front.* **5(5)** 673–682, https://doi.org/10.1016/j.gsf.2014.01.004.

Jayathilaka W M R, Dharmapriya P L, Kleinschrodt R and Spiering B 2022 Metamorphic evolution of charnockites across the inferred highland-Wanni boundary in Northeastern Sri Lanka; *J. Geol. Soc. Sri Lanka* **23(1)** 34–54.

Jonsson N F and Liu W 2020 Controls on cobalt and nickel distribution in hydrothermal sulphide deposits in Bergslagen, Sweden – Constraints from solubility modelling; *GFF* **142(2)** 87–95, https://doi.org/10.1080/11035897.2020.1751270.

Katz M B 1987 Graphite deposits of Sri Lanka: A consequence of granulite facies metamorphism; *Miner. Deposita* **22** 18–25, https://doi.org/10.1007/BF00204238.

Kawagucci S 2015 Fluid geochemistry of high-temperature hydrothermal fields in the Okinawa Trough; Subseafloor biosphere linked to hydrothermal systems: TAIGA Concept, pp. 387–403, https://doi.org/10.1007/978-4-431-54865-2_30.

Kay S M 1977 The origin of antiperthites in anorthosites; *Am. Mineral.* **62(9–10)** 905–912.

Kehelpannala K V W 1993 Structural evolution in the area surrounding the Kahatagaha–Kolongaha graphite mines, N–NW of Kandy, and the origin of vein graphite in Sri Lanka; *Ph.D. thesis*, The University of Mainz, Germany.

Kehelpannala K V W 1995 Origin of vein graphite: Another view; In: *Handbook on Geology and Mineral Resources of Sri Lanka, Second South Asia Geological Congress Colombo, Sri Lanka* (ed.) Dahanayake K, Geol. Surv. and Mines Bureau, Sri Lanka, pp. 95–104.

Kehelpannala K V W 1997 Deformation of a high-grade Gondwana fragment, Sri Lanka; *Gondwana Res.* **1** 47–68, https://doi.org/10.1016/S1342-937X(05)70005-8.

Kehelpannala K W 1999 Epigenetic vein graphite mineralization in the granulite terrain of Sri Lanka; *Gondwana Res.* **2(4)** 654–657, https://dl.nsf.gov.lk/handle/1/23401.

Kehelpannala K V W 2003 Structural evolution of the middle to lower crust in Sri Lanka; *J. Geol. Soc. Sri Lanka* **11** 45–86.

Keith M, Smith D J, Jenkin G R, Holwell D A and Dye M D 2018 A review of Te and Se systematics in hydrothermal pyrite from precious metal deposits: Insights into ore-forming processes; *Ore Geol. Rev.* **96** 269–282, https://doi.org/10.1016/j.oregeorev.2017.07.023.

Kirilova M, Toy V, Rooney J S, Giorgetti C, Gordon K C, Collettini C and Takeshita T 2018a Structural disorder of graphite and implications for graphite thermometry; *Solid Earth* **9(1)** 223–231, https://doi.org/10.5194/se-9-223-2018.

Kirilova M, Toy V, Timms N, Halfpenny A, Menzies C, Craw D, Beyssac O, Sutherland R, Townend J, Boulton C and Carpenter B M 2018b Textural changes of graphitic carbon by tectonic and hydrothermal processes in an active plate boundary fault zone, Alpine Fault, New Zealand; *Geol. Soc. London, Spec. Publ.* **453(1)** 205–223, https://doi.org/10.1144/SP453.1.

Kleinschrodt R 1994 Large-scale thrusting in the lower crustal basement of Sri Lanka; *Precamb. Res.* **66(1–4)** 39–57, https://doi.org/10.1016/0301-9268(94)90043-4.

Kleinschrodt R 1996 Strain localization and large-scale block rotation in the lower continental crust, Kataragama area, Sri Lanka; *Terra Nova* **8(3)** 236–244, https://doi.org/10.1111/j.1365-3121.1996.tb00752.x.

Kleinschrodt R and Voll G 1994 Deformation and metamorphic evolution of a large-scale fold in the lower crust: The Dumbara synform, Sri Lanka; *J. Struct. Geol.* **16(11)** 1495–1507, https://doi.org/10.1016/0191-8141(94)90028-0.

Kriegsman L 1991 Structural geology of the Sri Lanka basement – A preliminary review; In: *The Crystalline Crust of Sri Lanka, Part I. Summary of Research of the German-Sri Lankan Consortium* (ed.) Kröner A, Geol. Surv. Dept. Sri Lanka, Prof. Pap. **5** 54–68.

Kriegsman L M 1994 Evidence for a fold nappe in the high-grade basement of central Sri Lanka: Terrane assembly in the Pan-African lower crust?; *Precamb. Res.* **66(1–4)** 59–76, https://doi.org/10.1016/0301-9268(94)90044-2.

Kriegsman L M 1995 The Pan-African event in East Antarctica: A view from Sri Lanka and the Mozambique Belt;

Precamb. Res. **75(3–4)** 263–277, https://doi.org/10.1016/0301-9268(95)80010-F.

Kröner A 1991 African linkage of Precambrian Sri Lanka; *Geol. Rundsch.* **80(2)** 429–440, https://doi.org/10.1007/BF01829375.

Kröner A, Kehelpannala K V W and Kriegsman L M 1994 Origin of compositional layering and mechanism of crustal thickening in the high-grade gneiss terrain of Sri Lanka; *Precamb. Res.* **66(1–4)** 21–37, https://doi.org/10.1016/0301-9268(94)90042-6.

Kröner A, Kehelpannala K V W and Hegner E 2003 Ca. 750–1100 Ma magmatic events and Grenville-age deformation in Sri Lanka: Relevance for Rodinia supercontinent formation and dispersal, and Gondwana amalgamation; *J. Asian Earth Sci.* **22(3)** 279–300, https://doi.org/10.1016/S1367-9120(03)00060-9.

Kröner A, Rojas-Agramonte Y, Kehelpannala K V W, Zack T, Hegner E, Geng H Y, Wong J and Barth M 2013 Age, Nd–Hf isotopes, and geochemistry of the Vijayan Complex of eastern and southern Sri Lanka: A Grenville-age magmatic arc of unknown derivation; *Precamb. Res.* **234** 288–321, https://doi.org/10.1016/j.precamres.2012.11.001.

Kwiecińska B and Petersen H I 2004 Graphite, semi-graphite, natural coke, and natural char classification–ICCP system; *Int. J. Coal Geol.* **57(2)** 99–116, https://doi.org/10.1016/j.coal.2003.09.003.

Liew T C, Milisenda C C and Hofmann A W 1991 Isotopic contrasts, chronology of elemental transfers and high-grade metamorphism: The Sri Lanka Highland granulites, and the Lewisian (Scotland) and Nuk (SW Greenland) gneisses; *Geol. Rundsch.* **80** 279–288, https://doi.org/10.1007/bf01829366.

Liu W, Borg S J, Testemale D, Etschmann B, Hazemann J L and Brugger J 2011 Speciation and thermodynamic properties for cobalt chloride complexes in hydrothermal fluids at 35–440 C and 600 bar: An in-situ XAS study; *Geochim. Cosmochim. Acta* **75(5)** 1227–1248, https://doi.org/10.1016/j.gca.2010.12.002.

Liu W, Migdisov A and Williams-Jones A 2012 The stability of aqueous nickel (II) chloride complexes in hydrothermal solutions: Results of UV–Visible spectroscopic experiments; *Geochim. Cosmochim. Acta* **94** 276–290, https://doi.org/10.1016/j.gca.2012.04.055.

Lowenstern J B, Bergfeld D, Evans W C and Hunt A G 2015 Origins of geothermal gases at Yellowstone; *J. Volcanol. Geotherm. Res.* **302** 87–101, https://doi.org/10.1016/j.jvolgeores.2015.06.010.

Luque del Villar F J, Pasteris J D, Wopenka B, Rodas M and Fernández Barrenechea J M 1998 Natural fluid-deposited graphite: Mineralogical characteristics and mechanisms of formation; *Am. J. Sci.* **298** 471–498, https://hdl.handle.net/20.500.14352/57786.

Luque F J, Crespo-Feo E, Barrenechea J F and Ortega L 2012 Carbon isotopes of graphite: Implications on fluid history; *Geosci. Front.* **3(2)** 197–207, https://doi.org/10.1016/j.gsf.2011.11.006.

Luque F J, Huizenga J M, Crespo-Feo E, Wada H, Ortega L and Barrenechea J F 2014 Vein graphite deposits: Geological settings, origin, and economic significance; *Miner. Deposita* **49** 261–277, https://doi.org/10.1007/s00126-013-0489-9.

Madugalla T B N S, Pitawala H M T G A and Karunaratne D G G P 2014 Use of carbonatites in the production of precipitated calcium carbonate: A case study from Eppawala, Sri Lanka; *Nat. Resour. Res.* **23** 217–229, https://doi.org/10.1007/s11053-013-9222-8.

Malaviarachchi S P and Dharmapriya P L 2021 Trace element ratios hardly modify during extreme metamorphism of pelitic sediments as evidenced from the Highland Complex, Sri Lanka; *Lithos* **394** 106120, https://doi.org/10.1016/j.lithos.2021.106120.

Malaviarachchi S P, Satish-Kumar M and Takahashi T 2021 New Sr–Nd isotope data record juvenile and ancient crust-mantle melt interactions in the Vijayan complex, Sri Lanka; *J. Geol.* **129(2)** 233–253, https://doi.org/10.1086/714172.

Mathavan V and Fernando G W A R 2001 Reactions and textures in grossular-wollastonite-scapolite calc-silicate granulites from Maligawila, Sri Lanka: Evidence for high-temperature isobaric cooling in the meta-sediments of the Highland Complex; *Lithos* **59(4)** 217–232, https://doi.org/10.1016/S0024-4937(01)00057-3.

Migdisov A A, Zezin D and Williams-Jones A E 2011 An experimental study of Cobalt (II) complexation in Cl- and H2S-bearing hydrothermal solutions; *Geochim. Cosmochim. Acta* **75(14)** 4065–4079, https://doi.org/10.1016/j.gca.2011.05.003.

Milisenda C C, Leiw T C, Hofmann A W and Kröner A 1988 Isotopic mapping of age provinces in Precambrian high-grade terrains: Sri Lanka; *J. Geol.* **96** 608–615, https://doi.org/10.1086/629256.

Milisenda C C, Redmann M and Malango V 1994 A new occurrence of dendritic opal in south-eastern Zambia; *J. Gemmol.* **24(4)** 277–280.

Ortega L, Millward D, Luque F J, Barrenechea J F, Beyssac O, Huizenga J M, Rodas M and Clarke S M 2010 The graphite deposit at Borrowdale (UK): A catastrophic mineralizing event associated with Ordovician magmatism; *Geochim. Cosmochim. Acta* **74(8)** 2429–2449, https://doi.org/10.1016/j.gca.2010.01.020.

Ouzegane K, Guiraud M and Kienast J R 2003 Prograde and retrograde evolution in high-temperature corundum granulites (FMAS and KFMASH systems) from In Ouzzal terrane (NW Hoggar, Algeria); *J. Petrol.* **44(3)** 517–545, https://doi.org/10.1093/petrology/44.3.517.

Patten C G, Pitcairn I K and Teagle D A H 2017 Hydrothermal mobilisation of Au and other metals in supra-subduction oceanic crust: Insights from the Troodos ophiolite; *Ore Geol. Rev.* **86** 487–508, https://doi.org/10.1016/j.oregeorev.2017.02.019.

Petersen M D 1983 The use of the 'immobile' elements Zr and Ti in lithogeochemical exploration for massive sulphide deposits in the Precambrian pecos greenstone belt of northern New Mexico; *J. Geochem. Explor.* **19(1–3)** 615–617, https://doi.org/10.1016/0375-6742(83)90051-1.

Perera L R K 1987 Petrogenesis of granulite facies metamorphic rocks in Sri Lanka; *Unpublished M. Phil Thesis*, University of Peradeniya, 124p.

Pirajno F 1992 Alkali metasomatism and related mineral deposits; In: Hydrothermal mineral deposits: Principles and Fundamental Concepts for the Exploration Geologist, pp. 247–279.

Pirajno F 2012 *Hydrothermal mineral deposits: Principles and fundamental concepts for the exploration geologist*; Springer Science and Business Media.

Pitawala A and Lottermoser B G 2012 Petrogenesis of the Eppawala carbonatites, Sri Lanka: A cathodoluminescence

and electron microprobe study; *Miner. Petrol.* **105** 57–70, https://doi.org/10.1007/s00710-012-0193-y.

Pohl J R and Emmerann R 1991 Chemical composition of the Sri Lankan Precambrian basement; In: *The crystalline crust of Sri Lanka: Excursion guide for Geological Field Trip in Sri Lanka. Part I, Summary of research of the German-Sri Lankan Consortium* (Professional paper/Geological Survey Department; 5. IGCP project; 304), Ministry of Industries, Science and Technology, pp. 94–124, https://gfzpublic.gfz-potsdam.de/pubman/item/item_234287.

Prame W K B N 1991 Petrology of the Kataragama Complex, Sri Lanka: Evidence for high P–T granulite facies metamorphism and subsequent isobaric cooling; The crystalline crust of Sri Lanka, part 1, pp. 200–224.

Putnis A 2014 Why mineral interfaces matter; *Science* **343(7178)** 1441–1442, https://doi.org/10.1126/science.1250884.

Raase P and Schenk V 1994 Petrology of granulite-facies metapelites of the Highland Complex, Sri Lanka: Implications for the metamorphic zonation and the PT path; *Precamb. Res.* **66(1–4)** 265–294, https://doi.org/10.1016/0301-9268(94)90054-X.

Ruizggudo E, Putnis C V, Rodriguez-Navarro C and Putnis A 2012 Mechanism of leached layer formation during chemical weathering of silicate minerals; *Geology* **40(10)** 947–950, https://doi.org/10.1130/G33339.1.

Ruizggudo E, King H E, Patiño-López L D, Putnis C V, Geisler T, Rodriguez-Navarro C and Putnis A 2016 Control of silicate weathering by interface-coupled dissolution-precipitation processes at the mineral-solution interface; *Geology* **44(7)** 567–570, https://doi.org/10.1130/G37856.1.

Rumble D 2014 Hydrothermal graphitic carbon; *Elements* **10(6)** 427–433, https://doi.org/10.2113/gselements.10.6.427.

Sandiford M, Powell R, Martin S F and Perera L R K 1988 Thermal and baric evolution of garnet granulites from Sri Lanka; *J. Metamorph. Geol.* **6(3)** 351–364, https://doi.org/10.1111/j.1525-1314.1988.tb00425.x.

Santosh M, Tsunogae T, Malaviarachchi S P, Zhang Z, Ding H, Tang L and Dharmapriya P L 2014 Neoproterozoic crustal evolution in Sri Lanka: Insights from petrologic, geochemical and zircon U–Pb and Lu–Hf isotopic data and implications for Gondwana assembly; *Precamb. Res.* **255** 1–29, https://doi.org/10.1016/j.precamres.2014.09.017.

Schenk P M 1991 Ganymede and callisto: Complex crater formation and planetary crusts; *J. Geophys. Res.: Planets* **96(E1)** 15,635–15,664, https://doi.org/10.1029/91JE00932.

Schumacher R and Schmincke H U 1991 Internal structure and occurrence of accretionary lapilli – A case study at Laacher See Volcano; *Bull. Volcanol.* **53** 612–634, https://doi.org/10.1007/BF00493689.

Schumacher R, Schenk V, Raase P and Vitanage P W 1990 Granulite facies metamorphism of metabasic and intermediate rocks in the Highland Series of Sri Lanka; In: *High-temperature metamorphism and crustal anatexis*, Dordrecht, Springer, Netherlands, pp. 235–271, https://doi.org/10.1007/978-94-015-3929-6_10.

Sen S 1959 Structures of the porphyritic granite and associated metamorphic rocks of east Manbhum, Bihar, India; *Bull. Geol. Soc. Am.* **67(5)** 647–670, https://doi.org/10.1130/0016-7606(1956)67[647:SOTPGA]2.0.CO;2.

Shirey S B, Cartigny P, Frost D J, Keshav S, Nestola F, Nimis P, Pearson D G, Sobolev N V and Walter M J 2013 Diamonds and the geology of mantle carbon; *Rev. Mineral. Geochem.* **75(1)** 355–421, https://doi.org/10.2138/rmg.2013.75.12.

Sillitoe R H 2015 Epithermal paleosurfaces; *Miner. Depos.* **50(7)** 767–793, https://doi.org/10.1007/s00126-015-0614-z.

Silva K K M W 1987 Mineralization and wall-rock alteration at the Bogala graphite deposit, Bulathkohupitiya, Sri Lanka; *Econ. Geol.* **82(7)** 1710–1722, https://doi.org/10.2113/gsecongeo.82.7.1710.

Simpson C and Wintsch R P 1989 Evidence for deformation-induced K-feldspar replacement by myrmekite; *J. Metamorph. Geol.* **7(2)** 261–275, https://doi.org/10.1111/j.1525-1314.1989.tb00588.x.

Song Y, Griffiths T A and Zhao S and Abart R 2024 Myrmekite and antiperthite formation in weakly deformed granite: Chemical and crystallographic constraints on formation mechanisms; https://doi.org/10.2139/ssrn.4697295.

Su B X, Wang J, Cui M M, Wu Y, Pang K N, Malaviarachchi S P and Dharmapriya P L 2022 Element partitioning and Li–O isotope fractionation between silicate minerals and crustal-derived carbonatites and their implications; *J. Geophys. Res.: Solid Earth* **127(6)** e2022JB024563, https://doi.org/10.1029/2022JB024563.

Tani Y and Yoshida M 1996 The structural evolution of the Arena Gneisses and its bearing on Proterozoic tectonics of Sri Lanka; *J. Southeast Asian Earth Sci.* **14(3–4)** 309–329, https://doi.org/10.1016/S0743-9547(96)00067-0.

Tian Y, Etschmann B, Liu W, Borg S, Mei Y, Testemale D, O'Neill B, Rae N, Sherman D M, Ngothai Y and Johannessen B 2012 Speciation of nickel (II) chloride complexes in hydrothermal fluids: In situ XAS study; *Chem. Geol.* **334** 345–363, https://doi.org/10.1016/j.chemgeo.2012.10.010.

Touret J L R and Huizenga J M 2012 Fluid-rock interaction in retrograde granulites of the Southern Marginal Zone, Limpopo high grade terrain, South Africa; *Geosci. Front.* **5(5)** 673–682, https://doi.org/10.1016/j.gsf.2014.01.004.

Touret J L R, Huizenga J M, Kehelpannala K W and Piccoli F 2019 Vein-type graphite deposits in Sri Lanka: The ultimate fate of granulite fluids; *Chem. Geol.* **508** 167–181, https://doi.org/10.1016/j.chemgeo.2018.03.001.

Touzain P, Balasooriya N, Bandaranayake K and Descolas-Gros C 2010 Vein graphite from the Bogala and Kahatagaha–Kolongaha mines, Sri Lanka: A possible origin; *Can. Mineral.* **48(6)** 1373–1384, https://doi.org/10.3749/canmin.48.5.1373.

Vitanage P W 1972 Post-precambrian uplift and regional neotectonic movements in Ceylon; *24th Int. Geol. Congr., Sect.* **3** 642.

Vogel T A 1970 Albite-rich domains in potash feldspar; *Contrib. Mineral. Petrol.* **25(2)** 138–143, https://doi.org/10.1007/BF00389782.

Wada H, Tomita T, Matsuura K, Tuchi K, Ito M and Morikiyo T 1994 Graphitization of carbonaceous matter during metamorphism with references to carbonate and pelitic rocks of contact and regional metamorphisms,

Japan; *Contrib. Mineral. Petrol.* **118** 217–228, https://doi.org/10.1007/BF00306643.

White R W, Powell R and Holland T J B 2007 Progress relating to calculation of partial melting equilibria for metapelites; *J. Metamorph. Geol.* **25(5)** 511–527, https://doi.org/10.1111/j.1525-1314.2007.00711.x.

Wigley M, Dubacq B, Kampman N and Bickle M 2013 Controls of sluggish, CO_2-promoted, hematite and K-feldspar dissolution kinetics in sandstones; *Earth Planet. Sci. Lett.* **362** 76–87, https://doi.org/10.1016/j.epsl.2012.11.045.

Wijayananda N P and Jayawardena De S 1983 Some aspects of the geology of graphite mineralization in Sri Lanka, with particular reference to Kahatagaha–Kolongaha area; *Trans. Inst. Min. Metall.* **92** B93–98.

Wilson G C, Kilius L R and Rucklidge J C 1995 Precious metal contents of sulfide, oxide, and graphite crystals; determinations by accelerator mass spectrometry; *Econ. Geol.* **90(2)** 255–270, https://doi.org/10.2113/gsecongeo.90.2.255.

Yoshida M, Kehelpannala K V W, Hiroi Y and Vitanage P W 1990 Sequence of deformation and metamorphism of granulites of Sri Lanka; *J. Geosci. Osaka City Univ.* **33** 69–107.

Yuan G, Cao Y, Schulz H M, Hao F, Gluyas J, Liu K, Yang T, Wang Y, Xi K and Li F 2019 A review of feldspar alteration and its geological significance in sedimentary basins: From shallow aquifers to deep hydrocarbon reservoirs; *Earth-Sci. Rev.* **191** 114–140, https://doi.org/10.1016/j.earscirev.2019.02.004.

Yuguchi T and Nishiyama T 2008 The mechanism of myrmekite formation deduced from steady-diffusion modeling based on petrography: Case study of the Okueyama granitic body, Kyushu, Japan; *Lithos* **106(3–4)** 237–260, https://doi.org/10.1016/j.lithos.2008.07.017

Zhang Q Q, Gao X Y, Chen R X and Zheng Y F 2020 Granulites record the tectonic evolution from collisional thickening to extensional thinning of the Tongbai orogen in central China; *J. Metamorph. Geol.* **38(3)** 265–295, https://doi.org/10.1111/jmg.12522.

Corresponding editor: George Mathew